

Utah State University

DigitalCommons@USU

---

All Graduate Theses and Dissertations

Graduate Studies

---

5-1993

## Properties of Rigid Foams for Application as Materials for Light Weight Structures in Space

Huichen Chi  
*Utah State University*

Follow this and additional works at: <https://digitalcommons.usu.edu/etd>



Part of the [Physics Commons](#)

---

### Recommended Citation

Chi, Huichen, "Properties of Rigid Foams for Application as Materials for Light Weight Structures in Space" (1993). *All Graduate Theses and Dissertations*. 2099.

<https://digitalcommons.usu.edu/etd/2099>

This Thesis is brought to you for free and open access by the Graduate Studies at DigitalCommons@USU. It has been accepted for inclusion in All Graduate Theses and Dissertations by an authorized administrator of DigitalCommons@USU. For more information, please contact [digitalcommons@usu.edu](mailto:digitalcommons@usu.edu).



PROPERTIES OF RIGID FOAMS FOR APPLICATION AS MATERIALS  
FOR LIGHT WEIGHT STRUCTURES IN SPACE

by

Huichen Chi

A thesis submitted in partial fulfillment  
of the requirements for the degree

of

MASTER OF SCIENCE

in

Physics

Approved:

---

Dr. John R. Dennison  
Major Professor

---

Dr. Don L. Lind  
Committee Member

---

Dr. Jan J. Sojka  
Committee Member

---

Dr. James P. Shaver  
Dean of Graduate Studies

UTAH STATE UNIVERSITY  
Logan, Utah

1993

## ACKNOWLEDGMENTS

I first wish to thank my thesis advisor, Professor J. R. Dennison, for his guidance, support, and encouragement during the time that we have worked together. I am grateful to him for teaching and introducing me to the world of research in physics.

I also wish to thank my parents for their constant support. Without them, I would not have been able to finish my studies.

To Thiokol Corporation, I am grateful for Dean Lester and Michael Blair for their providing information of previous research and equipment in their research laboratory and for their financial support through a university IR&D grant.

To Professor J. Sojka, I am grateful for his advice about this project through our group meetings.

Finally, I would like to thank my fellow undergraduate students, especially M. Adams for his assistance in building the pressure box, and J. Humphries for setting up the optical tests.

Huichen Chi

## CONTENTS

iii

	Page
ACKNOWLEDGMENTS.....	ii
LIST OF TABLES.....	iv
LIST OF FIGURES.....	v
ABSTRACT.....	vii
I. INTRODUCTION.....	1
II. REVIEW OF UNDERSTANDING OF FOAM STRCUTURES.....	6
A. General Structure of Foams.....	6
B. Mechanical Properties of Foams.....	20
III. EXPERIMENTAL RESULTS.....	26
A. Foam Characterization.....	26
B. Structural Studies.....	48
C. Density Gradients.....	71
IV. ANALYSIS OF RESULTS.....	75
A. Summary of Foam Characteristics.....	75
B. Mechanical Properties.....	76
C. Effects of Applied Hydrostatic Pressure.....	77
V. PROPOSED FUTURE WORK.....	80
A. Alternate Foam Materials.....	80
B. Density Uniformity.....	81
C. Thermal Properties.....	85
D. Outgassing.....	86
VI. CONCLUSIONS.....	88
REFERENCES.....	90

## LIST OF TABLES

Table	Page
1. ICP Analysis of Polystyrene Foam Components.....	27
2. Polystyrene density.....	31
3. Porosity of polystyrene foam.....	39
4. Radii of curved foam surfaces.....	59
5. (a) Compression and (b) deflection tests of polystyrene foams.....	67

## LIST OF FIGURES

Figure	Page
1. Materials for innovative space structures.....	2
2. Space formed structural beams.....	3
3. Examples of closed cell and open cell foams.....	9
4. Structural model of homogeneous uniform foam.....	10
5. Example of a surface fractal.....	16
6. Small angle scattering setup.....	18
7. Deformation mechanics in foams.....	22
8. Example of cellular solids.....	23
9. Pressure box block diagram.....	33
10. Schematic of the gas handling system.....	34
11. Photograph of pressure box and gas handling system.....	35
12. Imbibition method: Comparison of penetration depth of foams with and without surfactant.....	43
13. Imbibition method: Comparison of different pressure differentials.....	44
14. Imbibition method: Saturation penetration depth versus pressure differentials.....	45
15. Permeability versus pressure differential using imbibition method.....	47
16. Micrograph of polystyrene foam.....	49
17. Photograph of polystyrene foam.....	50
18. Cell size distribution of polystyrene foams.....	51
19. Cell wall distribution of polystyrene foams.....	52

Figure	Page
20. Estimated available volume versus pressure differential.....	57
21. Compression of six polystyrene foam samples treated with pressure differentials.....	58
22. Pressure box tests: Anisotropy versus pressure differential.....	60
23. Setup of compression and deflection tests.....	61
24. Stress versus strain of compression and deflection tests.....	63
25. Compression test: Elastic collapse stress versus pressure differentials.....	64
26. Young's Modulus versus pressure differential.....	65
27. Compression test: (a) The strain under maximum applied loads (~4.1 MPa) and (b) the elastic fraction of total strain versus pressure differentials.....	66
28. Photographs of barrel-shaped distortions of polystyrene foams.....	68
29. Micrographs of six compressed polystyrene foam samples treated with pressure differentials from -1 to 5 atm.....	69
30. Deflection test: Ultimate strength versus pressure differential.....	72
31. Block diagram of apparatus for optical measurements of foams.....	74

## ABSTRACT

Properties of Rigid Foams for Application as Materials  
for Light Weight Structures in Space

by

Huichen Chi, Master of Science

Utah State University, 1993

Major Professor: Dr. John Robert Dennison  
Department: Physics

The mechanical and mesoscopic structural properties of rigid cellular foam made of polystyrene have been investigated. Basic properties (e.g., density, total and available porosity, permeability, surface area, isotropicity, and cell size and cell wall thickness distributions) were measured. In most cases, alternative methods were used to determine which methods were most appropriate for the type of samples we studied. Standard compression and deflection mechanical tests were performed. The stress-strain curves and related mechanical properties were found to agree with standard cellular structural models of open-cell foams.

We investigated the effects of small ( $\sim < 5$  atm) hydrostatic stress applied to foam samples for long periods of time ( $\sim$  one day). We observed large changes (up to a factor of three) in the stress-strain diagrams, Young's modulus, elastic collapse stress, ultimate strength, resilience, Poisson's ratio, permeability, penetration depth, and available porosity. Effects were most pronounced above 2 atm applied pressure differential, but

were observed even for 1 atm loads. Short-term exposure to loads up to ten times as large did not cause comparable changes. These changes were interpreted as resulting from observed changes in the mesoscopic structure occurring near the surface using standard cellular structural models.

This work was originally motivated by applications of foam as an inflating agent and structural component of fiber-epoxy composite tubular struts to be used in innovative space structures. The key recommendations of this study, regarding such applications, are to closely monitor the effects on the mechanical properties of polystyrene foam of: (1) cell structure and density inhomogeneities, and (2) pressure differentials which may be encountered during deployment and curing.

(100 pages)

## I. INTRODUCTION

This research has been motivated by the need to find appropriate foams for lightweight space structures. Traditional construction projects in the space environment use preformed components fabricated on earth and assembled in space. Flexibility in design is limited and the cost is high. The innovative space structures proposed by the Thiokol Corporation use foam-reinforced structures fabricated on location in space (Fig. 1). Foam was chosen to fill the strut to give it strength and rigidity, and to inflate the strut (Fig. 2). We have studied materials selection for such struts, which include the skin tube, polymer binder, and foam. The purpose of this research is to look at one component, foam. By studying certain properties and carrying out tests on some trial materials, we hope to determine how to choose the best foams for this application.

The struts must be rigid to minimize vibration and maintain dimensional tolerance, have low thermal expansion to withstand high temperature gradients in space, and have no negative effects on the other components of the struts or the space environment (e.g. out-gassing). Therefore, the most important properties are mechanical strength and rigidity. Other material properties, such as density and porosity, are studied primarily with regard to how they affect the mechanical properties.

The foam materials being considered as the best for Thiokol's application to struts are acetone-swelled polystyrene, urethane foams, and silica sol-gels. Polystyrene foam was chosen to be the first test material because it offers desirable properties as an innovative material for application as a lightweight structure in space. It is found to deploy well in a vacuum and it has a low density. Polystyrene is the material presently being used at Thiokol to develop deployment methods and characterize the composite foams.

In order to study the general structure and mechanical properties of foams, we reviewed physics theories applicable to cellular foams in section II, which provides insight into and allows prediction of the strength of these foams. In the study of the general

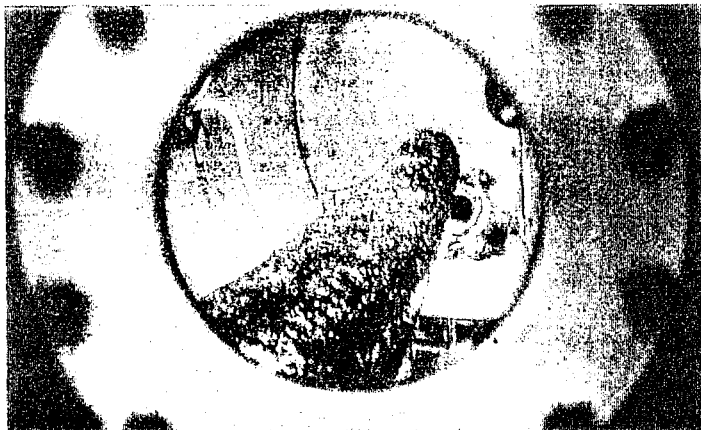
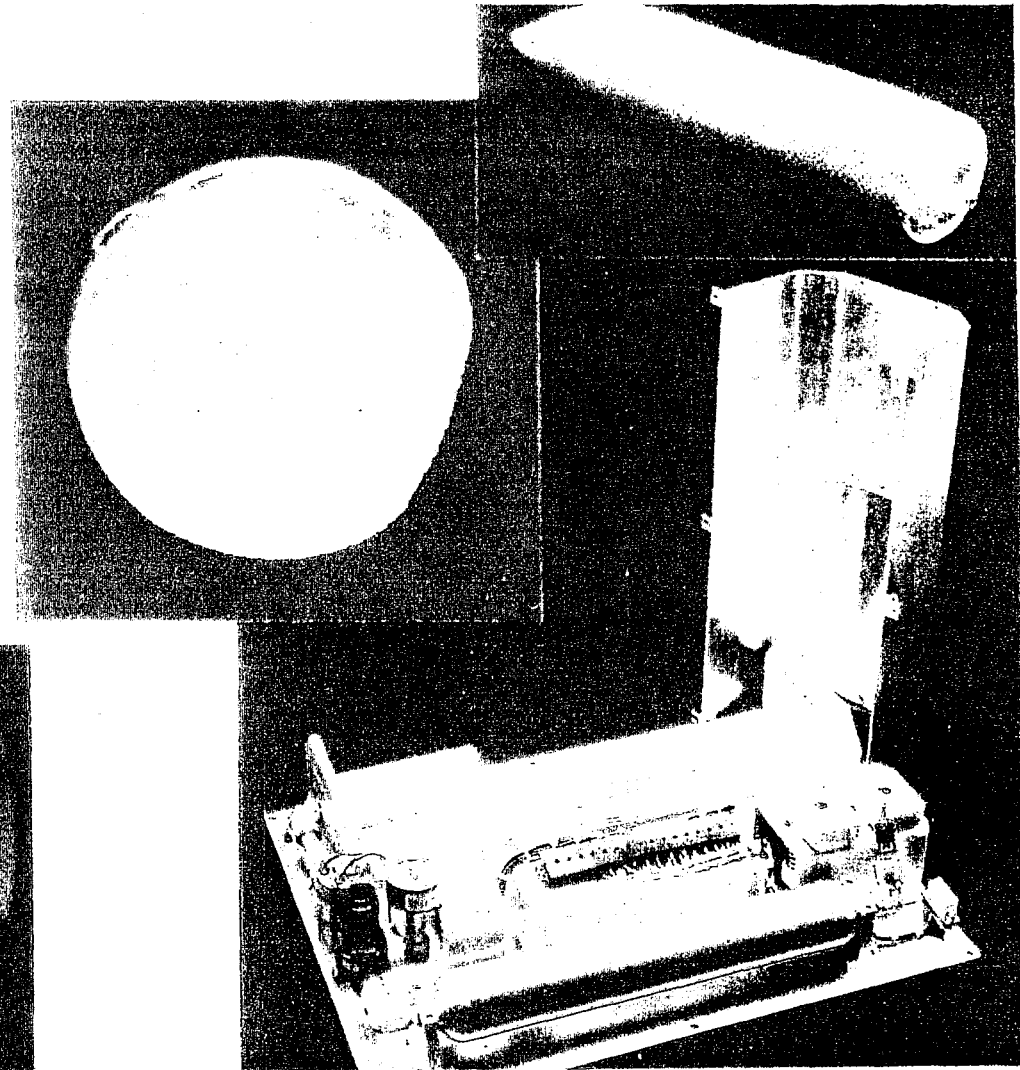
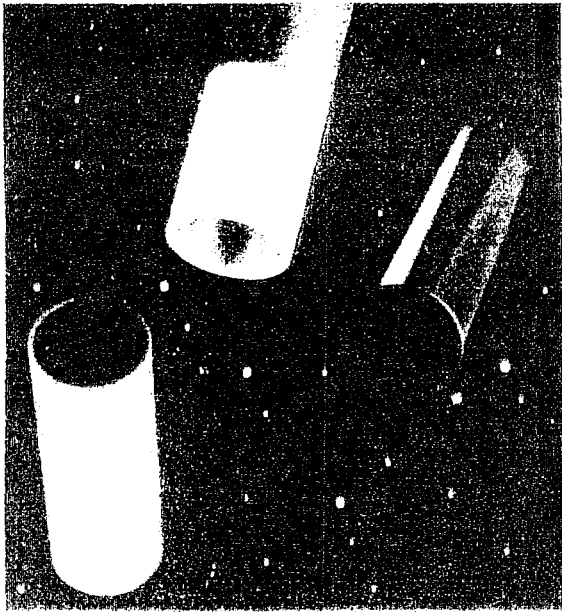


FIG. 1. Materials for innovative space structures. The apparatus shown at bottom right has been used at Thiokol to deploy foam filled struts as shown at top right (across section of the strut is shown at center. related projects at Thiokol include Gossamer foam structures (bottom left) and alternative struts (top left) (Reference from Thiokol Co.).

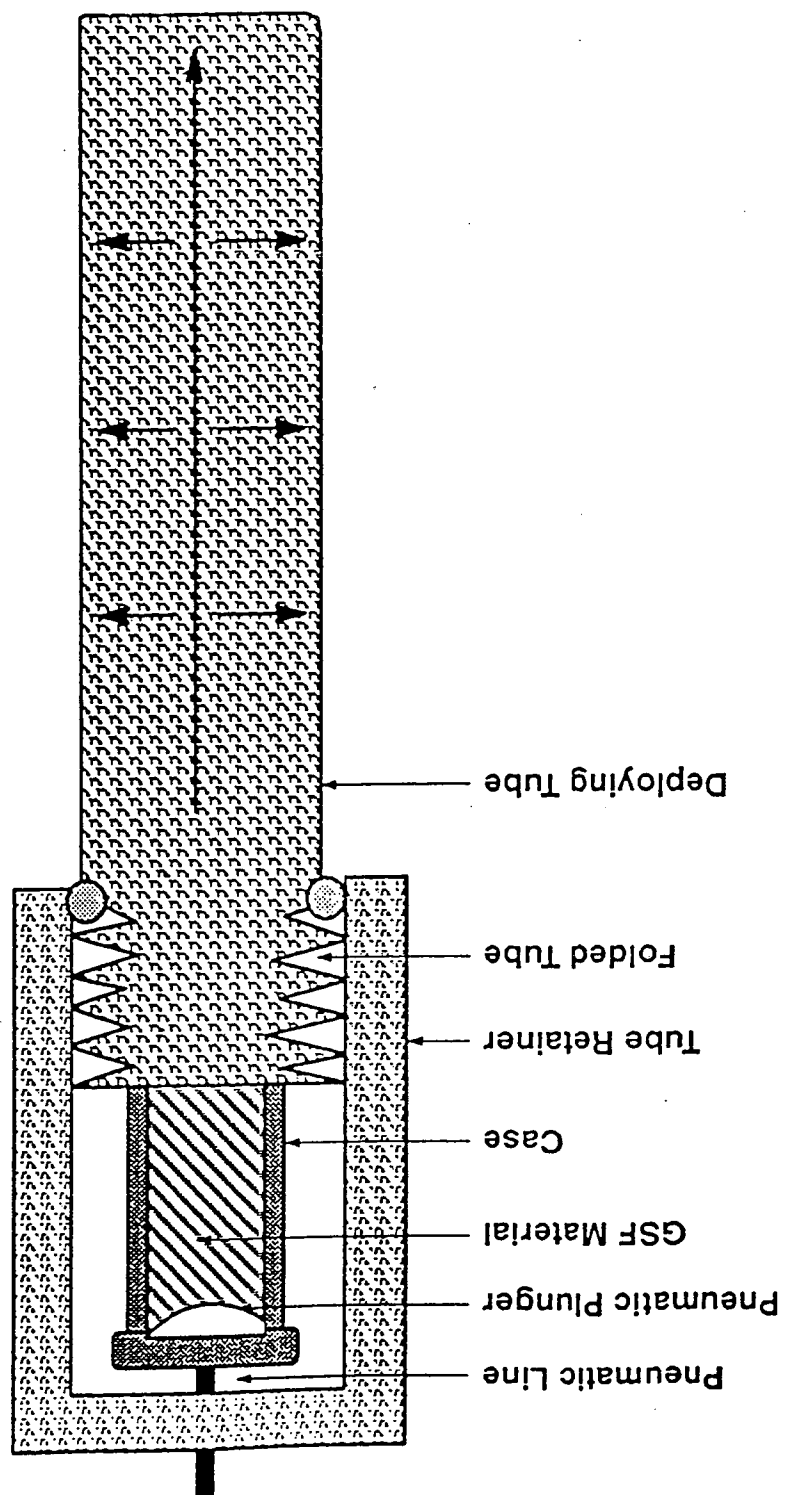


FIG. 2. Space formed structural beams. Laboratory scale heavy weight hardware.

structure of foams, density was found to be the most important aspect. Their light weight makes foams the ideal load-bearing materials in space. Useful properties related to density such as isotropy, open and closed cell structures, permeability, and porosity will be discussed. Applicable theories including fractal dimension and percolation theory will also be addressed in this section. Other essential characteristics of foam are their mechanical properties, which are also reviewed in section II. In a previous study of cellular solids and brittle foams, it was found that depending on the type and orientation of the external applied load, the foam cells underwent different types of deformation.<sup>1</sup> Therefore, the discussion of mechanical properties of foams was grouped into two categories: deformation by uniaxial loading and multiaxial loading.

Experimental measurements were developed to determine many of these properties as described in section III. Necessary test equipment for these measurements was determined for the chosen testing methods. Standard methods were used to study the polystyrene foam characteristics, which included density, porosity, surface area, and permeability. Testing equipment used for structural studies was either built or borrowed. In the measurements of cell wall structure of foam, a pressure box was designed and built. The measurements of mechanical tests were done at Thiokol's testing laboratory. We also started the measurement of the density gradient of both commercial polystyrene foam and man-made polystyrene foam provided by Thiokol.

The results of measurements are compared with the requirements for our applications in section IV. In the analysis of results, a summary of foam characteristics will be presented that is based on the goal of fulfilling the requirements of material selections as lightweight and strong materials. Also, determination of the mechanical properties of foam will be compared to the result of a previous work done by Ashby.<sup>1</sup>

A few additional measurements of foams as further research will be proposed in section V. Alternate foam materials such as polyurethane and aerogels were selected and

some of their properties will be compared to the properties of polystyrene foams. The density uniformity of polystyrene foam will be better understood by further tests. Other properties considered useful are thermal properties and outgassing of foams.

Finally, the conclusions of this research will be presented. We will review our results on the basic properties of rigid polystyrene foam with emphasis on the mechanical properties and will discuss how our results relate to current theories of the mesoscopic structure of foams. At the conclusion of this research, the following questions regarding our particular application for foams will also be addressed: (1) Which foams are appropriate for our applications in lightweight space structures? (2) What did we learn about the material selections process? (3) Are our evaluation methods and criteria applicable to other potential foams? (4) Will the same evaluation methods be appropriate for material selections for the other components of the struts? (5) How could the evaluation process be improved? (6) Do theories help predict useful material properties?

## II. REVIEW OF UNDERSTANDING OF FOAM STRUCTURES

In order to study the general structure and mechanical properties of foam, physics theories applicable to foams will be reviewed. These theoretical bases will provide insight into and allow prediction of the strength of foam.

In previous work on the foam structures,<sup>2</sup> foams were characterized as a skeletal structure surrounding cells. For example, coffee cups and crash padding of an aircraft cockpit are foam products in our everyday lives. A cell is a small component, an enclosed space. Porous materials are assemblies of cells with solid edges or faces, packed together so that they fill space. A cellular solid is one made up of an interconnected network of solid struts or plates that form the edges and faces of cells. The cells are polyhedra that pack in three dimensions to fill space; such three-dimensional cellular materials are called foams.

The density of foam is related to the porous property, conductivity, and strength of the foams. The low density, low thermal conductivity, and crushing ability of polymer foams make them ideal load-bearing materials for structures in space. It is crucial to study both the density of the foams and the cell wall strength to determine the best material for the struts. In the applications of foams, the structural properties depend on the density and on the direction of loading. These two important aspects will be discussed in the following sections. The properties of foam structures considered below are the relative density, isotropy, open versus closed cell structure, permeability, porosity, and fractal dimension.

### A. General Structure of Foams

#### 1. Density

The most important aspect of the structure is the relative density  $r$ , which is the ratio of the density of the foam to the density of the solid from which the foam is made.

$$r = \frac{\rho_f}{\rho_b} \quad (1)$$

where  $\rho_f$  is the density of foam, and  $\rho_b$  is the bulk density. The bulk is the solid from which the cell walls are made. Polystyrene bulk density is 1.05 g/cm<sup>3</sup>.<sup>1</sup> Polymeric foams for cushioning, packaging, and insulation have relative densities between 0.05 and 0.2. When the cell-wall density of foam is unknown, it can be estimated with an error less than 15% based on relative density of the foam alone.

## 2. Isotropy

Isotropy implies that the structure and properties of a foam exhibit no preferred direction. When the individual cells are uniaxial, the structural properties are isotropic, but when cells are elongated, the properties depend on alignment of the cells. Almost all man-made foams are anisotropic. However, their cells can still be described by one of the regular polyhedron, the tetrakaidecahedron.<sup>1</sup> The structure will be discussed in the next section.

We found it necessary to study both the isotropic foams and the anisotropic foams. Studies of cork structure demonstrated the importance of the anisotropic nature of some foams. Different strengths in the longitudinal and perpendicular directions of the cork make it a good sealing material for wine bottles. This thesis starts with the research of commercial polystyrene foams, and will present possible experimental processes for the anisotropic foams.

## 3. Open and closed cell

A more important designation than the shape of the cells is the distribution of the solid between the edges and the cell walls. Some foams are closed-cell foams (such as a soap foam), others are open-cell foams (for example, sponges). Of course, some foams may have both closed and open cells. If the solid of which the foam is made is contained in the cell edges only, the foam is called open-celled. If the faces are solids too, each cell is sealed

off from its neighbors and it is called closed-celled (Fig. 3).

In the closed-cell foams, the solid material is distributed in little plates which form the faces of the cells. The walls are of approximately uniform thickness and are much thinner than the edges. The edges have uniform cross section along their length, thickening only when they meet each other. On the other hand, the solid material is distributed in little beams that form the cell edges for the open-cell foams. The walls are retracted into the edges and the structure consists of a framework of struts in space.

Different models have been suggested to describe the distribution of the directions of the cell edges in any cross-sectional area. The proper choice of equations depends on the dimensionality of the structure and on whether a foam has open or closed cells.

The simplest model for a foam structure includes identical spheres uniformly distributed in a solid matrix.<sup>1</sup> The open-cell and closed-cell foams are modeled in two dimensions by a honeycomb, of which the edge length is  $l$  and the cell wall thickness is  $t$  (Fig. 4). Assuming low relative density (that is  $t \ll l$ ), the relative density of an open-cell foam is given by

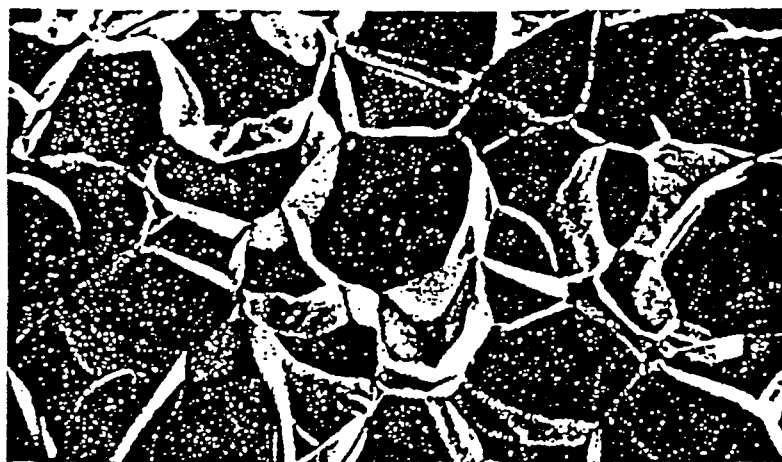
$$\frac{\rho_f}{\rho_b} \sim \left(\frac{t}{l}\right)^2 \quad (2)$$

where the bulk material is contained in beams of length  $l$  and cross sections of  $t$  by  $t$ . The relative density of a closed-cell foam is then

$$\frac{\rho_f}{\rho_b} \sim \frac{t}{l} \quad (3)$$

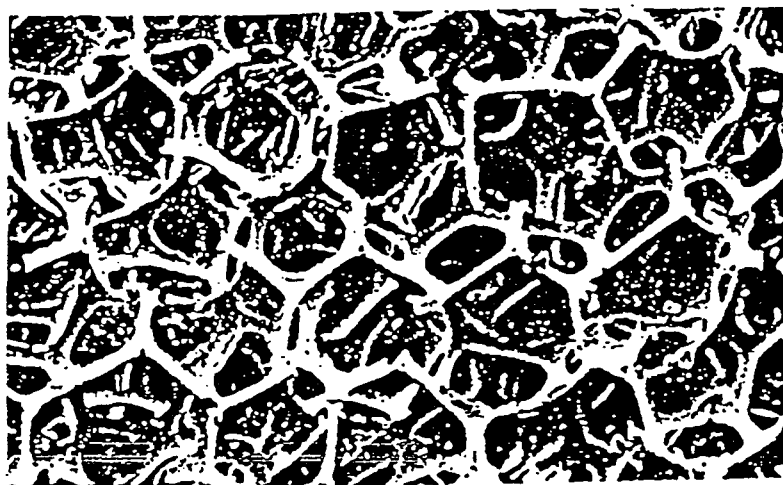
where the bulk material is contained in plates of thickness  $t$  and area  $l$  by  $l$ . The proportionality constant depends on the details of the cell shape.

Polymers are foamed by introducing gas bubbles into the liquid monomer or hot polymer, allowing the bubbles to grow and stabilize, and solidifying the whole thing by



1 mm

Closed cell



1 mm

Open cell

FIG. 3. Example of closed cell and open cell foams (after reference 1).

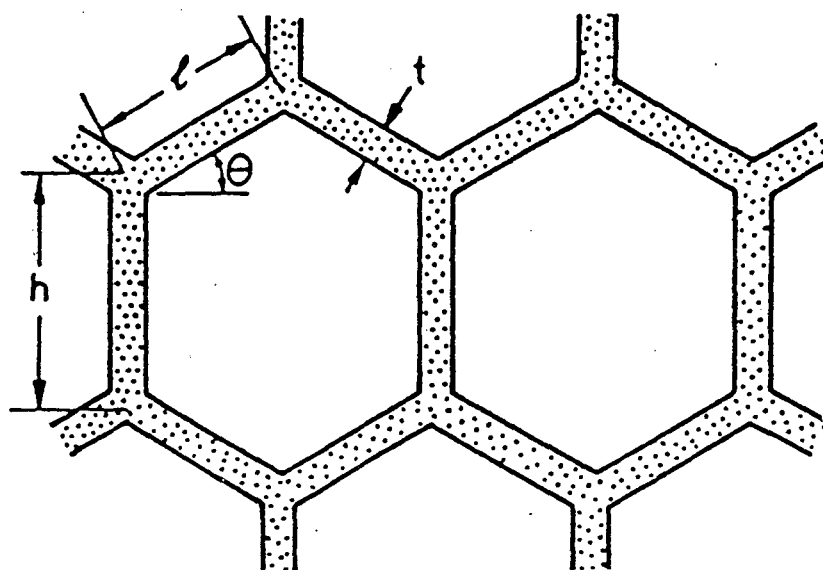


FIG. 4. Structural model of homogeneous uniform foams.

cross-linking or cooling.

A typical polymer foam is characterized by closed cells of a roughly uniform size. But, even those with closed-cell faces behave structurally like open-celled foams because surface tension draws much of the solid material into the cell edges during manufacture, leaving a thin skin framed by thicker edges. When the foaming process places restrictions on the flow of the polystyrene, the cells get elongated in the direction of free flow. Such anisotropy of structure is common in low-density foams.

The distinction between open and closed cells is obvious from the micrographs, but it can also be determined from the permeability of the foam to a gas or a liquid.

#### 4. Permeability

Permeability is the property of a porous material which characterizes the ease with which a fluid may flow through the material. It is defined from an empirical relation demonstrated by Darcy in 1856.<sup>3</sup> If  $v$  is the volume of fluid crossing unit area per unit time under the pressure gradient  $dp/dx$ , for small  $v$ ,

$$\frac{k}{\eta} \times \frac{dp}{dx} = v \quad (4)$$

where  $k$  is the permeability and  $\eta$  is the coefficient of viscosity of the fluid. It is found<sup>3</sup> that Darcy's law holds for  $R$  less than 5. A Reynolds number is defined as  $R = \frac{av\rho}{\eta}$  (where  $a$  is the average pore size and  $\rho$  is the fluid density). To relate the permeability and the fundamental properties of the medium, Kozeny's equation is a good approximation to the permeability of materials with few closed cells.<sup>3</sup> That is

$$k = \frac{1}{5} \left( \frac{p^3}{(1-p)^2 s^2} \right) \quad (5)$$

where  $p$  is the available porosity, and  $s$  is the total surface area of the particles in a unit volume of the medium.

## 5. Porosity

In the study of the structure of cellular solids, important parameters are porosity, cell size, and cell shape. Mechanical properties depend on porosity and cell shape and only weakly on the cell size. We also need to study the porosity of foams to determine the permeability, as discussed above. Porosity is also an important parameter in describing transport properties (e.g. mass, heat, and electrical conductivity).

Total porosity is the fraction of volume of voids per unit total volume, given as

$$P_{total} = \frac{V_{voids}}{V_{foam}} \quad (6)$$

From the relation of closed volume and available volume, we can derive that total porosity is related to the relative density by

$$P_{total} = 1 - \frac{\rho_f}{\rho_b} \quad (7)$$

where  $P_{total}$  is the total porosity,  $V_{voids}$  is the volume of all voids, and  $V_{foam}$  is the total volume of foam.

Available porosity (the ratio of open cell volume to total foam volume) is known as the open cell fraction, and is less than the total porosity. The trapped volume is the closed cell volume, which is the total volume excluding the cell walls and open cell volume.

Porosity can be measured by a great variety of methods.<sup>4</sup> A straightforward method is to measure the bulk volume of a piece of porous material and compact the body so as to destroy all its voids, and to measure the difference in volumes.

Another way to determine the porosity is by photographing a section of the porous medium with a microscope, and then use a planimeter. The pore size distribution can thus be determined. Such visual methods of porosity determination have been applied by Zavodovskaya (1937) to porcelain, by Dallmann (1941) to bread, and by Verbeck (1947) to

concrete.<sup>5</sup> Difficulties will be encountered if the porous medium is dispersed. A dye can be added to the impregnating materials so as to make the voids more visible.

Density methods include measuring the outside dimensions and weighing the piece of material before and after crushing. A volumetric displacement method (use a non-wetting fluid, e.g. mercury) measures the change in weight of a soaked porous medium outside the liquid or measures the volume of liquid soaked into the foam.

A typical method to measure porosity is the gas expansion method. It is a direct measurement of the volume of gas contained in the open pore space. This can be achieved either by evacuating the air out of the specimen, or by enclosing the specimen of known bulk volume and a certain amount of gas in a container of known volume under pressure, then connecting this with an evacuated container of known volume. The new pressure of the system permits one to calculate the accessible volume and available porosity from the ideal gas law. The gas expansion method was originally employed by Washburn and Bunting (1922).<sup>5</sup>

One proposed method for the study of porosity is nuclear magnetic resonance (NMR).<sup>6</sup> The application of NMR spin-lattice relaxation measurements of water contained in porous solids was investigated in the article as a possible tool for the determination of pore structure. In principle, water contained in a pore will relax faster than bulk water. The relaxation is partly caused by the interaction of the solid surface with fluid molecules near the surface. Thus the relaxation rate provides direct information about the surface-to-volume ratio. Therefore, the pore sizes in a porous structure can be determined. According to the fast diffusion theory, there is a local averaging of the molecular relaxation over regions, having dimensions of the order of this diffusion length.<sup>7</sup> Numerical laplace inversion of the relaxation data provides information about the size distribution of the pores, spatially averaged by diffusion over a length scale of several microns.

Another method for measuring the porosity uses ultrasonics. Ultrasonic

characterization of porosity in composite materials and ceramics by time delay spectrometry has been shown in papers.<sup>8,9</sup> In order for this method to be effective, the material pore size was assumed. Each pore in these materials was considerably smaller than typical ultrasonic longitudinal inspection wavelengths, and provides only negligible scattering. The characterization was done with optical microscopy, radiography, and ultrasonic techniques. All of the techniques delineated the porosity distribution in varying degrees and different ways. Porous study specimens with controlled void volume percentages, pore sizes, and distributions have been produced using careful moisture and thermal management techniques. Measurements of ultrasonic attenuation have been made at multiple frequency values utilizing time delay spectrometry (TDS).<sup>10,11</sup> Existing models have been used to calculate apparent porosity volume percentages and pore sizes from the ultrasonic data.

## 6. Fractal Dimension

Recent developments in theoretical physics have allowed descriptions of the open structural nature of a material in terms of the fractal dimension. Compact bulk material is three-dimensional, while a material made of very thin membranes (e.g. soap bubbles) can be said to be two-dimensional. Intuition suggests that foams, made of thick walls and beams, have "dimensions" somewhere between two and three; the fractal dimension provides a well-defined theoretical concept to quantify just such a phenomenon.

Obviously, the fractal dimension, which is related to such key structural properties as cell size distribution and cell wall structure, may provide a valuable parameter for theories characterizing the mechanical properties of foams. Relative density has been found to be an essential parameter in describing the mechanical properties of foams. However, density alone can not distinguish between a foam with few large cells and relatively thick cell walls and a foam with many smaller cells and relatively thin cell walls. These two extremes obviously can have drastically different mechanical properties. Not only can

the fractal dimension distinguish these two cases, but it provides a natural method to describe distributions of cell sizes and wall thicknesses.

The fractal dimension of a lignite coal has been measured using small-angle x-ray scattering.<sup>12</sup> The fractal dimension was determined to be  $2.56 \pm 0.03$ . Fractal dimensions are used to model important properties of foams. For instance, a scaling relation was developed for the fracture strength of a porous material or random network near the percolation threshold.<sup>13</sup> Involved parameters are porosity, elasticity and coherence length, and fractal dimension. The diffusion of gases through foams with nonuniform cell sizes was described using fractal models by Kimball and Frisch.<sup>14</sup> The fractal dimension and ways to measure it will be discussed in this section.

Fractal dimensions have been studied for over 50 years, although the term "fractal" was not invented until 1975 by Mandelbrot.<sup>15</sup> The geometry of many natural objects ranging in the size from the atomic scale to the size of the universe may be of the fractal structure. A fractal is a shape made of parts similar to the whole in some way, a property which is called self-similarity (Fig. 5).

The fractal dimension  $d$  is defined<sup>16</sup> by

$$N(r) = \left(\frac{r}{r_0}\right)^d \quad (8)$$

where  $N(r)$  is the quantity obtained by measuring a fractal material with a measuring gauge of size  $r_0$ . For example,  $N(r)$  can be the number of particles of radius  $r_0$  which lie within a sphere of radius  $r$  centered on an arbitrary particle.

Small angle x-ray scattering (SAXS) and small angle neutron scattering (SANS) have been found to be especially well suited for studying the fractal nature of disordered systems, including polymers, aggregates of particles, and gels.<sup>17</sup>

In discussions of the use of small-angle scattering to study fractals, it is important to consider two types of fractal systems: mass fractals and surface fractals. Mass fractals,

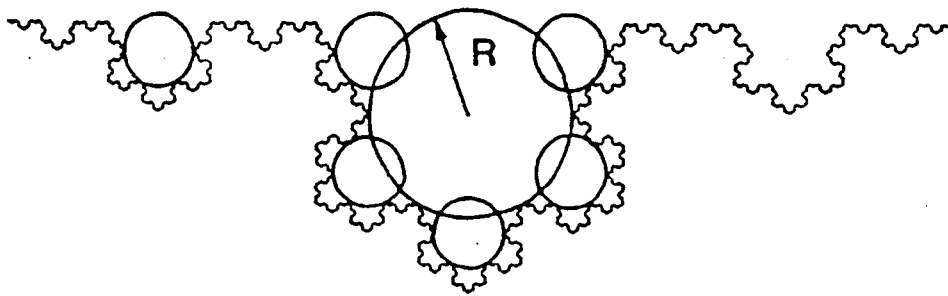


FIG. 5. Example of a surface fractal. The jagged curve is the self-similar fractal surface. The spheres indicate the measurement of surface area as a function of the size of the sphere.

which are typically aggregates of subunits, are structures for which the mass inside a spherical surface with radius  $r$  and with its center at a point in the mass-fractal center is given by

$$M_{mass}(r) \sim r^d \quad (9)$$

On the other hand, a surface fractal is a region with mass-fractal dimension  $d_{mas}$  that is embedded in a space of Euclidean dimension  $D=3$  and is bounded by a fractal surface with surface-fractal dimension  $d$ .<sup>18</sup> The fractal properties extend throughout a mass-fractal system but are bound only of fractal systems. Surfaces demonstrate fractal properties only on length scales much smaller than the diameters of the mass fractal aggregates. Many properties of fractal systems can often be described by quantities that are proportional to a power of another quantity.<sup>17</sup>

In particular, the intensity  $I(q)$  of the SAXS and SANS of many disordered systems (including polymers, aggregates of particles, and aerogels) has been found to be proportional to a negative power of

$$q = \frac{4\pi}{\lambda} \sin\left(\frac{\theta}{2}\right) \quad (10)$$

where  $q$  is the momentum transfer,  $\lambda$  is the x-ray wavelength, and  $\theta$  is the scattering angle (refer to Fig. 6).

Shaefer et al. have used light and x-ray scattering to study the colloidal aggregates of silica particles.<sup>19</sup> Consider a general distribution of particles in the material with density  $\rho(r)$  describing a mass fractal of fractal dimension  $d$ . The differential cross section is

$$\sigma(q) \sim \frac{M\Gamma(d-1) \sin\left(\frac{\pi(d-1)}{2}\right)}{q^d} \quad (11)$$

where  $M$  is the mass of the material, and  $\Gamma(d-1)$  is the gamma function.<sup>20</sup>

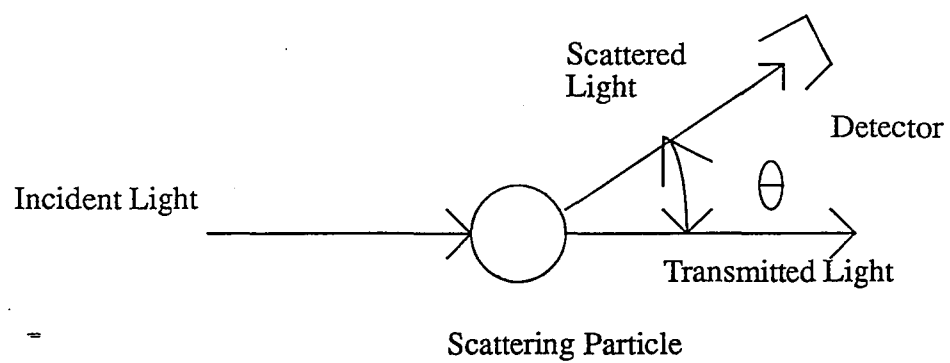


FIG. 6. Small angle scattering setup.

If the solid is bounded by a fractal surface, the density distribution is proportional to three-dimensional power of the cube size. The density-density correlation function

$$\rho(r) = V - nr^{3-d} \quad (12)$$

where  $V$  is the volume of the scattering sample,  $n$  is the proportionality constant of the fractal surface, and  $d$  is the Hausdorff dimension of the surface.<sup>18</sup> The Hausdorff dimension is the fractal dimension measured under the condition that any detail smaller than the unit of measurement is not counted. Using this result and carrying through the calculations, the surface contribution to the differential cross section was found as

$$\sigma(q) \sim \frac{\pi N \Gamma(5-d) \sin\left(\frac{\pi(d-1)}{2}\right)}{q^{6-d}} \quad (13)$$

The slope of a log-log plot of the scattering intensity versus scattering angle determines the surface fractal dimension.<sup>20</sup> Note that this relation is linear (and  $d$  well defined) only over a range of length scales for which the material is self-similar (that is for which it can be described as a fractal).

Fractal dimensions of surface fractals can sometimes be measured by molecular adsorption on fractal surfaces. The number of molecules to cover the set is a function of the size of molecules. Reference 20 describes the considerable research done to determine the small scale surface roughness (0.4 nm to the pore size) of porous solids, usually expressed as a surface fractal dimension. This is normally determined using either molecular tiling via the change in surface area as a function of the adsorption probe size, or small angle X-ray or neutron scattering. When the roughness of the surface is on the order of the film thickness, the volume of the vapor adsorbed is measured. If the pore size is on the order of the film thickness, the pore size distribution can be determined. Plotting the log of the film surface area as a function of the adsorbed film volume, the surface fractal dimension can be

obtained from the slope of the linear region. In the nonlinear region, the pore size distribution can be determined.

## B. Mechanical Properties of Foams

In order to use foam as a material in load-bearing structures, it is important to understand its mechanical properties. In a previous study of cellular solids and brittle foams, it was found that depending on the type and orientation of the externally applied load, the foam cells undergo different types of deformation.<sup>21</sup>

Consider a foam sample under uniaxial compression, in the two-dimensional model. The axial beams will be under pure compression, while the oblique beams will have some bending stresses induced in them (see Fig. 8). We will start with the discussion of uniaxial loading on foam.

### 1. Deformations by uniaxial loading

Analyzing foam is difficult: the cell walls form an intricate three-dimensional network which distorts during deformation in ways which are hard to identify. We begin the study of foam structure by gaining a basic understanding of the mechanics of two-dimensional honeycombs (see Fig. 4).

If the honeycomb is compressed in-plane (the plane of Figures), the cell walls at first bend, giving linear elastic deformation. At lower strains than  $\epsilon_D$ , the cell walls collapse and the internal volume of the cells disappears. The densification occurs on the steep part of the stress-strain curve just below  $\epsilon_D$ .

An analysis of the physical mechanisms responsible for the homogeneous deformation of three-dimensional foams has been well established.<sup>21</sup> It relates a well defined mechanism with each mode of deformation. For elastomeric foams, four different deformation modes were identified: linear elasticity, nonlinear elasticity, elastic collapse, and various manners of fracture.

At low strains, elastic foams deform as linearly elastic bodies, followed by a plateau of constant-stress deformation. This plateau is further extended because of the crushing together of neighboring cells to a region of densification (Fig. 7).<sup>1</sup> Thus, the elastic moduli of these materials, which are assumed as orthotropic substances, are related to the bending stiffness of the elements composing the cell walls, whereas the elastic collapse of these materials is caused by elastic buckling of these elements and the plastic collapse is conducted by plastic hinges formed inside these elements (Fig. 8).<sup>1</sup> In the region of elastic buckling the material exists in two states at almost the same stress: the linear-elastic and the densified states. As the strain is increased the beams thicken at almost constant stress until the entire material has reached the dense state.

The magnitude of the initial modulus, i.e. the slope of the first part of the stress-strain curve, is related to the relative density of foam.<sup>22, 23</sup> If a force  $F$  is applied vertically to an open-cell foam, the nonvertical beams will deflect by

$$\delta = \frac{c_1 F l^3}{12 E_s I} \quad (14)$$

where  $c_1$  is a factor which depends on the cell geometry,  $E_s$  is the Young's modulus of the solid cell wall material,  $I$  is the second moment area, and  $l$  is the cell dimension. Ashby's article showed there are simple relations between the relative Young's modulus (defined as  $E/E_s$ ) and relative density and between the relative stress and relative density. The relation of the first modulus and relative density can be calculated to be

$$\frac{E}{E_s} = c_2 \left( \frac{\rho}{\rho_s} \right) \quad (15)$$

where  $\rho_s$  is the density of the solid, and  $c_2$  is a proportionality constant, which was found to be one for many polymer foam materials.

In similar research,<sup>24</sup> a simple power-law relationship between various

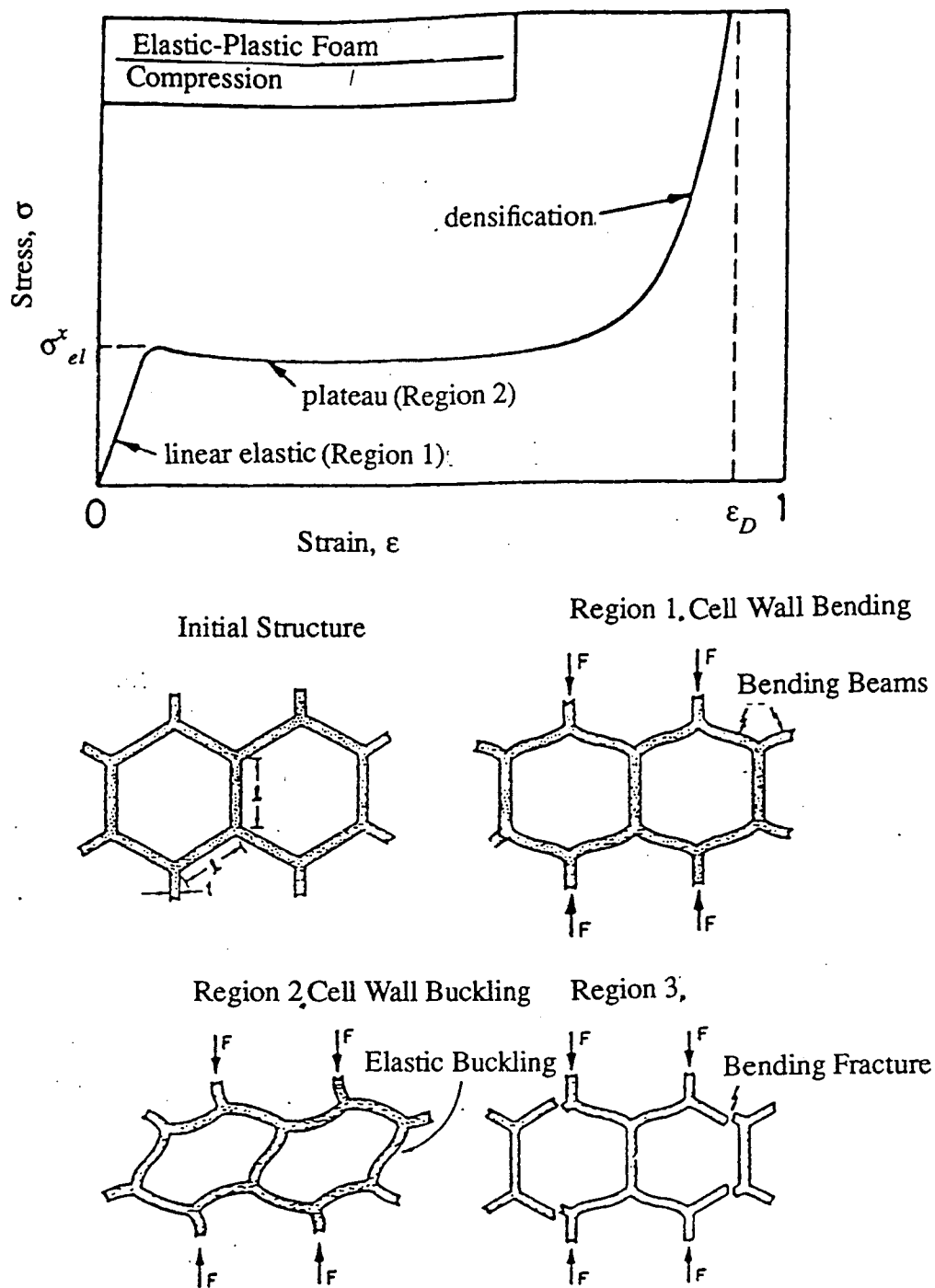
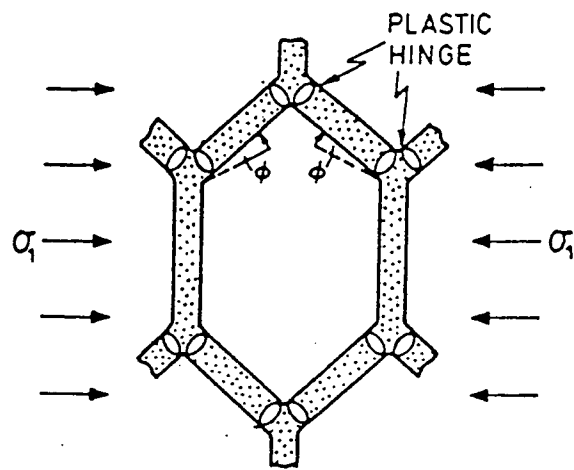
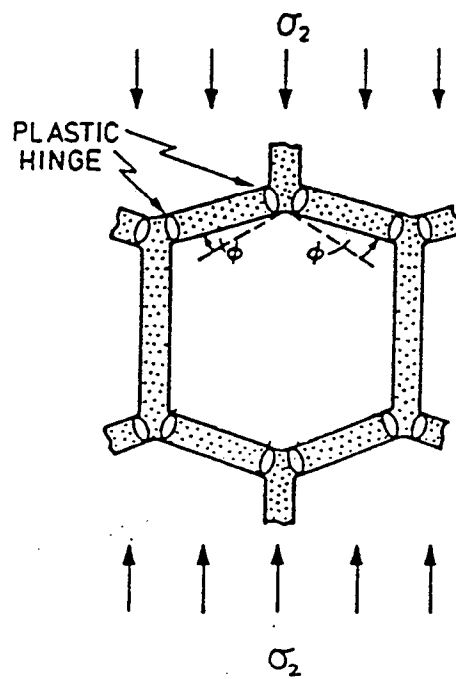


Fig. 7. Deformation mechanics in foams. In the linear elastic region (Region 1) cell wall bending occurs. Beginning at the plastic yield stress  $\sigma_{el}^x$  for elastic-plastic foams, there is a plateau in the stress-strain curve where cell walls buckle (Region 2), yield, and then fracture (Region 3). Finally densification of the foam occurs as the cell walls are crushed together.



(a)



(b)

Fig. 8. Example of cellular solids under uniaxial stress: (a) axial stress, (b) oblique stress.

mechanical properties and density for polymer foams has been indicated. For instance, the Young's modulus relates density by

$$E \sim \rho^n \quad (16)$$

where  $n=3$  for closed-cell foams, and  $n=2$  for open-cell foams. In all cases, the values of  $n$  were higher for stiffness than strength. The slope in a linear log-log plot of relative stress and relative density determines  $n$ .

Other proposed models used to fit experimental stress-strain data were purely empirical relations of stress to either engineering or Hencky's strain.<sup>25</sup> These models were presented in the study of compression data of bread and polyurethane foams.

Model 1:

$$\sigma = \frac{c_1 \epsilon}{(1 + c_2 \epsilon) (c_3 - \epsilon)} \quad (17)$$

Model 2:

$$\sigma = c_1 \left( \frac{\epsilon}{c_2 - \epsilon} \right)^{c_2} \quad (18)$$

Model 3:

$$\sigma = \frac{c_1 (1 - e^{-c_2 \epsilon})}{c_3 - \epsilon} \quad (19)$$

Model 4:

$$\sigma = c_1 \epsilon^{c_2} + c_3 \epsilon^{c_4} \quad (20)$$

where  $\sigma$  is the stress, and  $\epsilon$  is the strain.

In the first three models,  $c_1$  was a scale factor with unit of stress, which represented

the stress level before densification. The parameter  $c_2$  was dimensionless, and has different meaning in different models. Also,  $c_3$  was dimensionless and described the densification strain level.

The fourth model has a different structure. Parameters  $c_1$ ,  $c_3$  had stress units, and  $c_2$ ,  $c_4$  were dimensionless. The first term represented the elastic yielding nature of the impact sponge and the second was related to its densification.

A recent report<sup>25</sup> showed the fit of the four models to compression data of bread and polyurethane foams, and the fourth model was identified as superior.

## 2. Deformation of foam by biaxial and multiaxial loads

It has been observed that tensile and compressive stresses result in failures of beams of the cells, which are oriented parallel to the direction of external load.<sup>21</sup> Different types of deformations caused by different types and orientations of the external applied load on the foam cells have been studied. An early paper<sup>21</sup> indicated that a polystyrene foam subjected to biaxial loading failed by the maximum principal stress criterion, and it suggested a rectangular failure surface. In a more recent study of the failure mode of foams, the author introduced a model of the elliptic paraboloid failure surface.<sup>21</sup> This newer model is valid for both anisotropic and isotropic brittle cellular foams under multiaxial loading. However, it will not be discussed in detail in this thesis.

### III. EXPERIMENTAL RESULTS

In this section, experimental measurements were developed to determine many properties as described in section I. Necessary test equipment for these measurements was determined for the chosen testing methods. Standard methods were used to study the polystyrene foam characteristics, which include density, porosity, surface area, and permeability. The measurements of cell wall structure of foam were designed; a pressure box was designed and built; the measurements of mechanical tests were made in Thiokol's testing laboratory.

#### A. Foam Characterization

##### 1. Material selection and sample preparation

Polystyrene foams were chosen to be the first test material because they deploy well in vacuum, and they are lightweight materials. These properties make them ideal load-bearing structures in space. The compositions of three different commercial polystyrene foams have been tested by inductively coupled plasma (ICP) analysis at the USU Soil Science Laboratory to determine trace element concentrations. These polystyrene samples include a bulk sample, a block of white foam, and a block of green foam. Table 1 shows that these samples all have the same trace elements (mostly Na, Al, and Zn), but with different concentrations. However, the primary elements in organic compounds (C, O and H) were not tested by ICP. The green foam differs from the white foam primarily by the dye, which does not affect the tests we performed. Therefore, we chose the white polystyrene foam as the sample tested for all subsequent measurements. The melting point of polystyrene foam used was found to be about 135 to 140 degrees C. Alternate materials are discussed in section V. A.

We choose to study samples of commercial polystyrene foam rather than use foam prepared by Thiokol. The Thiokol foam density, pore size distribution, homogeneity, and isotropicity varied significantly for different deployment methods and even from run to

Table 1. Trace analysis of commercial polystyrene foams by ICP analysis.

(where &lt; indicates element below the detection limit)

Element	Al	B	Ca	Cd	Co	Cr	Cu	Fe	K	Mg	Mn
Concentration	mg/kg	---	--%-	---	---	mg/kg	----	----	-%	-----	---
Bulk Chip	27	4.4	0.03	<	<	2	4.5	23	<	0.01	<
White foam	25	4.8	0.03	<	<	3	4.5	21	<	0.01	<
Green foam	21	8.0	0.03	<	<	3	4.7	14	<	0.01	<

Element	Mo	Na	Ni	P	Pb	S	Se	Sr	Zn
Concentration	---	mg/kg	----	--%-	mg/kg	--%-	-----	mg/kg	-----
Bulk Chip	<	91	<	<	<	<	3	0.8	113.4
White foam	<	259	<	0.01	<	<	3	3.4	9.0
Green foam	<	154	<	0.01	<	<	5	3.5	7.0

run under controlled conditions; this made a systematic characterization of the material and mechanical properties difficult. The commercial foam was found more homogeneous and isotropic than the Thiokol foams, but similar in other respects. The commercial foam density was somewhat lower than the typical Thiokol foams. The mean (number-average) molecular weights of the commercial and Thiokol foams were measured to be  $1.52 \cdot 10^5$  g/mole and  $1.77 \cdot 10^5$  g/mole, respectively, using high pressure liquid chromatography (Varian 5000) employing a size-exclusion column (Polymer Laboratories,  $300 \cdot 7.5$  mm,  $5 \mu$  particle size). The polydispersities were 1.94 and 2.02, respectively.

Because of the plastic property of commercial polystyrene foam, it is difficult to cut the foam accurately without crushing the cell walls. Different methods were tried. The most uniform shape of foam was obtained by using a band saw. The error in measuring the dimensions of the block that fits in the pressure box was less than one millimeter for ~5% volume uncertainty. Cutting the foam does cause damage to the cell wall structure, as is evidenced by the curvatures induced by applied hydrostatic pressure (section III. B. 2). However, this damage does not extend too far in from the surface. Measurements of the extent of open cell (penetration depth) using the imbibition method (section III. A. 5) showed little difference between cut and uncut surfaces.

## 2. Properties of polystyrene foam-Density

Since the relative density characterizes the cell wall strength, the most important property of the foam in determining its mechanical properties is the relative density. The relative density is the ratio of the density of the foam to the density of the solid from which the foam is made (usually called "bulk" or "neat" density). A foam with a smaller relative density is typically better as a lightweight structure component material than a denser material.

In the study of the relative densities, we used different experimental methods to measure the densities of bulk and foam. Gravimetric, compression, and dissolution

methods were used to study bulk density. The gravimetric, Archimedes', and microscopy methods were used to determine foam density.

The most direct method is to measure the volume and mass of a piece of foam. An electronic balance (Ohaus, model E400I) with an accuracy of 0.01 g was used. The density of foam determined by the gravimetric method was  $0.032 \pm 0.002 \text{ g/cm}^3$ . The primary source of uncertainty was the volume measurement.

The Archimedes' method includes three steps: First, measure the height of the water in the beaker and its mass; second, float the foam on the water, measure the height increase of the water, and weigh the beaker and foam again; third, apply pressure on the foam until it is totally immersed in water and then measure the mass and water level increase.

By balancing the buoyancy force and applied force, the volume of water displaced by bulk and closed cells can be calculated. The foam density can be determined by the following equations:

$$V_w = \frac{m_f}{\rho_w} \quad (21)$$

where  $V_w$  is the volume of water displaced by foam,  $m_f$  is the mass of foam, and  $\rho_w$  is the density of water (assumed to be  $1 \text{ g/cm}^3$ ). Therefore,  $\rho_f$  is the density of foam, which is

$$\rho_f = \frac{V_w \rho_w}{V_f} \quad (22)$$

where  $V_f$  is the volume of foam. The polystyrene foam density was measured by using Archimedes' method to be  $0.030 \pm 0.002 \text{ g/cm}^3$ . The primary source of uncertainty resulted from volume measurements.

The gravimetric method for the bulk density is the same as for the foam density. The bulk density was  $1.06 \pm 0.02 \text{ g/cm}^3$  by this method.

In the dissolution method, methylene chloride ( $\text{CH}_2\text{Cl}_2$ ) was used to dissolve the

foam so that all voids could be eliminated. To make sure that no bubbles are trapped in the polystyrene when it is cured, a known mass of polystyrene foam is dissolved, and the solution is centrifuged and then put under vacuum. After the solvent completely evaporated, the test tube containing the polystyrene was filled with water. The masses of water with bulk polystyrene and of water only (filled to the same level) were compared. From this, the bulk density under STP (at room temperature and one atm) was  $0.57 \pm 0.03 \text{ g/cm}^3$ . This is much smaller than the gravimetric result and suggests that some bubbles were still in the bulk.

The other method used to determine bulk density was compression. A block of foam with known initial volume and mass was compressed with a hand press and the volume of the pressed foam was measured. Only when enough pressure is applied to break all cell walls is this measurement accurate. The result obtained was  $0.25 \pm 0.08 \text{ g/cm}^3$ . In this case, not all voids were removed. After the external force was removed, the foam elastically recovered (see Table 2).

The foam density can also be estimated based on microscopy measurements (see section III.B.1) with average cell wall thickness  $t$  and average cell radius  $r_0$ . If we assume uniform-walled spherical cells

$$\frac{\rho_f}{\rho_b} = \frac{V_b}{V_f} = \frac{(4\pi r_0^2) \frac{t}{2}}{\frac{4}{3}\pi r_0^3} = \frac{3t}{2r_0} \quad (23)$$

Using this method the foam density was found to be  $0.06 \pm 0.03 \text{ g/cm}^3$ . The poor agreement suggests the approximation of cell geometry used here is not accurate.

### 3. Property of foam-porosity

The porosity of foam characterizes the strength of a cell network and the transport properties such as mass, heat, and electrical transport. Total porosity is the ratio of volume of voids to the total volume. Different methods have been developed to measure porosity,

Table 2. Polystyrene density: (a) bulk density, (b) foam density.

Method	Measured Value g/cm <sup>3</sup>	Random Error g/cm <sup>3</sup>	Primary Source of Uncertainty
Gravimetric	1.06	0.02 (2%)	volume measurement
Compression	0.25	0.08 (30%)	volume measurement
Dissolution	0.57	0.03 (5%)	volume measurement
Tabulated Density	1.05	---	---

Method	Measured Value g/cm <sup>3</sup>	Random Error g/cm <sup>3</sup>	Primary Source of / Uncertainty
Gravimetric	0.030	0.002 (5%)	volume measurement
Archimedes	0.030	0.002 (8%)	volume measurement
Microscopic	0.06	0.03(50%)	cell wall dimension
Tabulated Density	0.032	---	---

such as the gravimetric, dissolution, microscopy, NMR, and ultrasonic methods for total porosity. In our research, the methods used were the gravimetric, dissolution, and microscopy methods. The NMR and ultrasonic methods have been used on other materials such as ceramics instead of foams. They were described in the review section (section II.A), but no results were obtained for our samples.

The most direct method is to measure the bulk density of a piece of foam. By knowing the bulk density from the density measurements and the foam density, total porosity can then be obtained. This method gave  $93 \pm 5\%$  total porosity.

The dissolution method measures the volume of polystyrene before and after dissolution. It was described in the density measurement; the total porosity was  $97 \pm 10\%$ .

Another way to determine the porosity is by photographing a section of porous material with a microscope, and then use a planimeter. A dye was added so as to make the voids more visible. Using this microscopic method, the cell size and cell wall thickness distributions can also be determined. Therefore, the volume of total voids and the volume of foam can be estimated by assuming a spherical shape of the voids. The total porosity of polystyrene foam obtained by the microscopic method was  $95 \pm 28\%$ .

A typical method to measure the available porosity is the gas expansion method. It is a direct measurement of the volume of gas contained in the open pore space. This can be achieved either by evacuating the air out of the foam, or by enclosing a foam sample of a certain volume in a container (the pressure box) (Fig. 9) which has a known volume.

Connect the pressure box with another container (gas handling system, GHS) (Fig. 10) of known volume, then fill in the GHS with a certain amount of nitrogen. After the valve between pressure box and GHS is opened (Fig. 11), the balanced pressure of the system permits one to calculate from ideal gas law the gas volume that was originally in the porous material. The initial amount of gas is proportional to  $P_i V_{\text{GHS}}$ , where  $P_i$  is the initial pressure

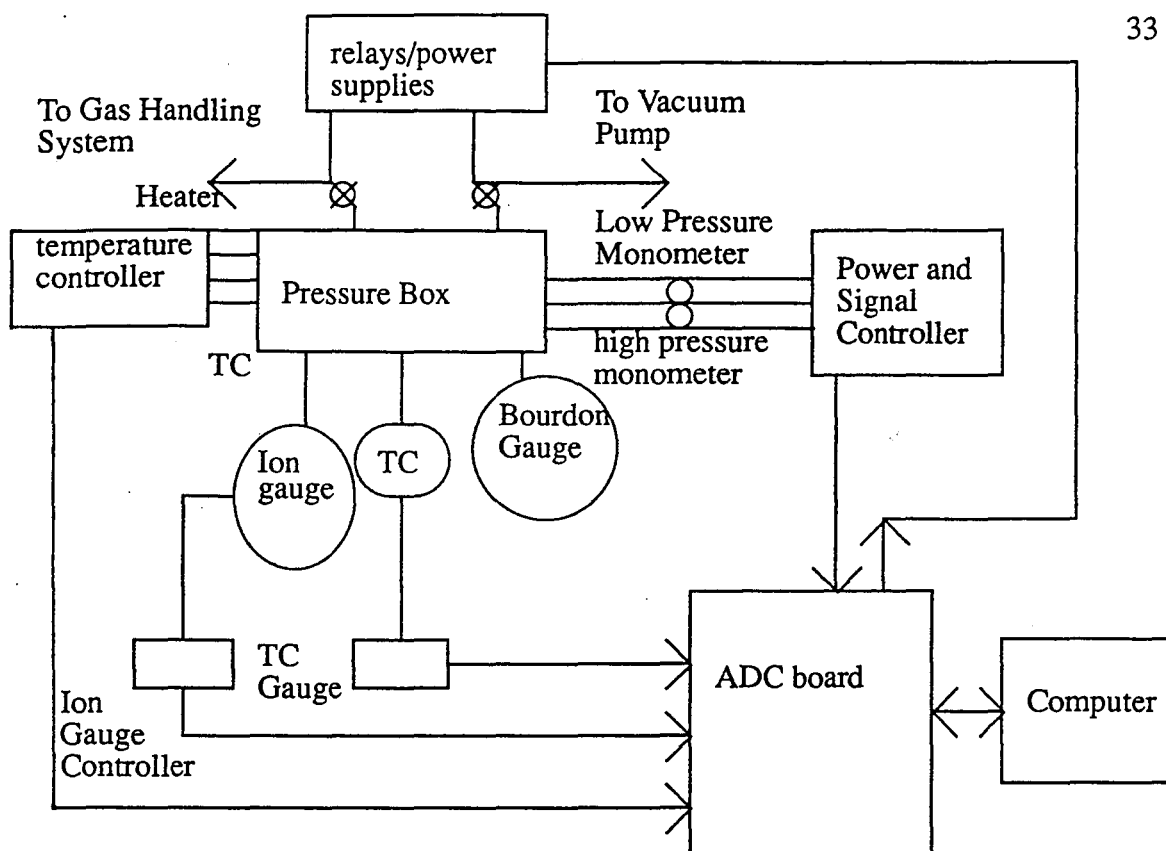


FIG. 9. Pressure box block diagram.

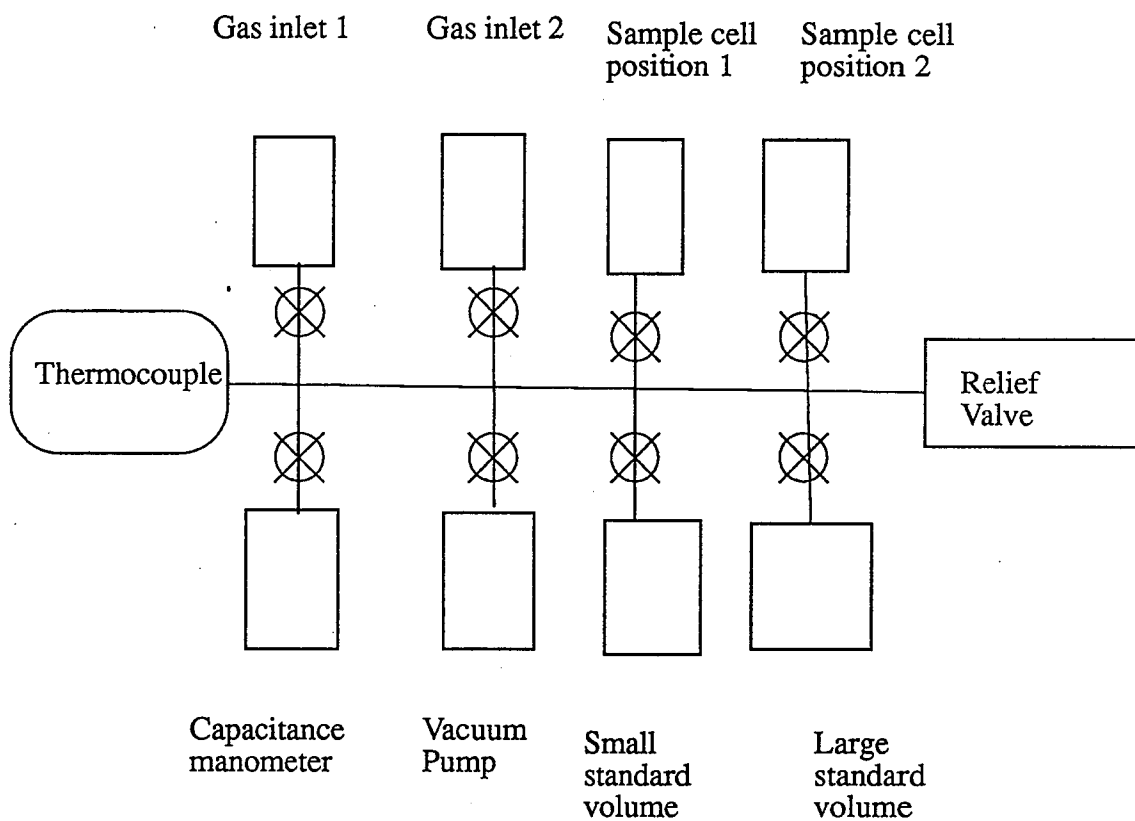


FIG. 10. Schematic of the gas handling system.

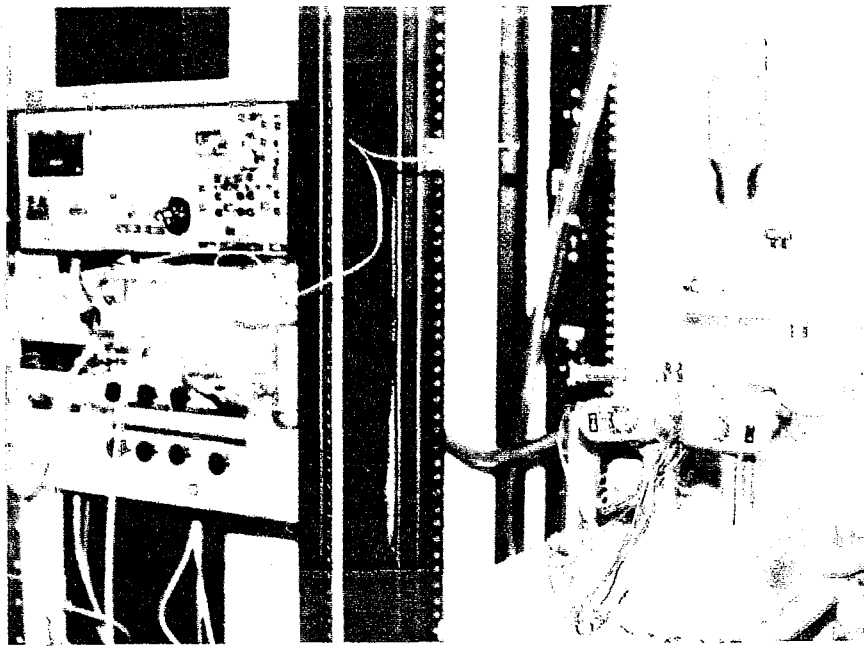


FIG. 11. Photograph of pressure box and gas handling system.

and

$$V_{GHS} = V_{ssv} + V_{lsv} + V_m \quad (24)$$

where  $V_{GHS}$  is the total volume of gas handling system,  $V_{ssv}$  is the small standard volume,  $V_{lsv}$  is the large standard volume, and  $V_m$  is the volume of manifold. The volume in the pressure box can be written as

$$V_{total} = V_b + V_c + V_a + V_{space} \quad (25)$$

where  $V_b$  is the volume of bulk polystyrene in the foam sample,  $V_c$  is the closed cell volume of foam,  $V_a$  is the available volume or open cell volume,  $V_{space}$  is the rest of the unoccupied volume in the pressure box. Apply the tabulated value of bulk density  $\rho_b$  into

$$V_b = \frac{m_f}{\rho_b} \quad (26)$$

After the valve is opened we have

$$P_i V_{GHS} = P_f (V_{GHS} + V_a + V_{space}) = P_f (V_{GHS} + V_{total} - V_b - V_c) \quad (27)$$

where  $P_f$  is the final pressure. This can be used to determine  $V_c$ . Then  $V_a$  is found from the measured total volume of the foam sample  $V_f$  as

$$V_f = V_c + V_a + V_b \quad (28)$$

The total volume of voids can be calculated by

$$V_{voids} = V_{total} - V_b - V_{space} = V_c + V_a \quad (29)$$

The total porosity is  $V_{\text{voids}} / V_f$  and the available porosity is  $V_a / V_f$ . Using this method, the total porosity is  $95 \pm 4\%$ , and the available porosity is  $1.5 \pm 0.3\%$ . The uncertainty is mostly from the measurement of the volume of pressure box.

Another way of measuring the porosity is the imbibition method. The imbibition method measures the change in mass of a soaked foam outside the liquid and the volume of liquid that was soaked up. Let

$$\Delta m = m_{(f+w)} - m_f \quad (30)$$

where  $m_{(f+w)}$  is the total mass of the soaked foam. Assume the volume of the open cells is very small compared to the total foam volume. The penetration depth of the imbibing liquid is

$$x = \frac{\Delta m}{A_f \rho_w} \quad (31)$$

where  $A_f$  is the total surface area of the foam sample block, and  $\rho_w$  is the density of the imbibing liquid. The available porosity will be

$$P_a = \frac{\left(\frac{\Delta m}{\rho_w}\right)}{V_f} \quad (32)$$

Also, the trapped volume will be

$$V_c = V_f - V_b - \frac{\Delta m}{\rho_w} \quad (33)$$

The available porosity obtained by this method was  $2.3 \pm 0.07\%$ . The trapped volume was  $30 \pm 1 \text{ cm}^3$  out of  $40 \pm 2 \text{ cm}^3$  of total foam volume (75% of total volume).

An innovative method used for the study of porosity of foam is the Archimedes' method. The foam sample of known mass and volume was immersed in water and forced

(by an applied weight) totally under the water level. Take the density of water to be  $1\text{g/cm}^3$ . Assume the ratio of the foam volume to available volume is equal to the ratio of the foam available surface area to total surface area.

$$1 - \frac{A_f^0}{A_f} = \frac{V_a}{V_f} \quad (34)$$

where  $A_f^0$  is the surface area of foam without the open cells.

In order to find  $V_a$ , we need to calculate the rise of water level  $x$  after the foam was forced into the water (since this change will be very small, the uncertainty in displacement is the major source of error in this method). The buoyancy force is balanced by the gravitational force produced by trapped volume. For

$$V_a = \frac{V_f - xA_b - xA_f}{\left(\left(\frac{xA_f}{V_f}\right) + 1\right)} \quad (35)$$

using  $x(A_b - A_f^0) = V_f - V_a$ , where use was made of Eq. 26, and  $A_b$  is the cross area of the beaker which contains foam sample and water. The available porosity is given by the definition

$$P_a = \frac{V_a}{V_f} \quad (36)$$

From these relations we found the total porosity was  $96 \pm 8\%$ , the available porosity was  $16 \pm 10\%$ , and the trapped volume of a unit weight was calculated to be  $30 \pm 2\text{cm}^3/\text{g}$  out of  $33 \pm 2\text{cm}^3/\text{g}$  (91% of total volume).

Generally speaking, the results obtained from different methods for the total and available porosity and trapped volume all agree with each other except for the dissolution method (see Table 3). The inaccuracy of data from dissolution method is mostly caused by the existence of persistent voids. The results showed that most of the polystyrene foam

Table 3. Porosity of polystyrene foams: (a) total porosity, (b) available porosity.

Method	Measured Value%	Random Error (relative uncertainty%)	Primary Source of Precision
Gravimetric	93	5 (5%)	volume of bulk
Dissolution	97	10 (10%)	volume of bulk
Microscopy	95	28 (30%)	cell wall dimensions
Archimedes	96	8 (8%)	volume of bulk
Pressure-volume curve	95	4 (4%)	volume of pressure box

Method	Measured Value%	Random Error (relative uncertainty%)	Primary Source of Precision
Imbibition	2.30	0.07 (3%)	available volume
Archimedes	16	10 (60%)	foam volume measurement
Pressure-volume curve	1.5	0.3 (20%)	volume of pressure box

consists of voids in the form of closed cells.

#### 4. Foam property-surface area

To help characterize the porosity and outgassing, it is necessary to measure the surface area of the foam. Two methods, the BET method and vapor pressure isotherms, have been considered.

The multimolecular adsorption theory of Brunauer, Emmett, and Teller, referred to as the BET method, has occupied a central position in adsorption studies.<sup>26</sup> This is because this method yields a useful two constant equation from which surface areas and approximate heats of adsorption can be readily calculated. The specific surface area of a solid is defined as the surface area per unit mass. The monolayer capacity is defined as the quantity of adsorbate that would be required to cover the adsorbent with a monomolecular layer only. The specific surface and the monolayer capacity are related by

$$\Sigma = 0.269 \times \sigma_m \times v_m \quad (37)$$

where  $\sigma_m$  is the area in square angstroms which one adsorbed molecule would occupy in the completed monolayer, and  $v_m$  is the volume which one adsorbed molecule would occupy in the completed monolayer. The BET equation is

$$v = \frac{v_m \times c \times p}{(p_0 - p) \times (1 + ((c - 1) \times \frac{p}{p_0}))} \quad (38)$$

where  $v$  is the volume adsorbed at relative pressure,  $c$  is a constant characteristic of the absorbate-absorbent pair,  $p_0$  is the saturation vapor pressure, and  $p/p_0$  is the relative pressure.

This equation is capable of describing the adsorption isotherms. By knowing that a clear surface is thermodynamically unstable to adsorption because the surface tension decreases with increasing adsorbate particle density, the adsorption isotherm can be obtained by plotting the surface strain with respect to the adsorbate vapor pressure. The value of  $v_m$  can be calculated from the slope of the BET isotherm. Based on the BET method done at the USU Water Research Laboratory, the total specific surface area of polystyrene foam was  $5.4 \pm 0.3 \text{ m}^2/\text{g}$  (this is the surface area of the available volume only  $A_f - A_f^0$ ). For comparison, note that high surface area powders such as MgO smoke or exfoliated graphite have specific surface areas of 2 to  $50 \text{ m}^2/\text{g}$ , soils have specific surface areas of 50 to  $250 \text{ m}^2/\text{g}$ , and sol-gels and aerogels have extremely high specific surface areas of 100 to  $1000 \text{ m}^2/\text{g}$ .

### 5. Property-permeability

Permeability is the property of a porous material that characterizes the ease with which a fluid may flow through the material. The imbibition method and BET adsorption isotherm were used to measure the permeability of foam.

The imbibition method was described in detail in the section on porosity measurements. In the permeability measurements, a foam sample was immersed in water containing a dye. The foam sample was weighed before it was immersed, and again after a week. The penetration depth is found by

$$T = \frac{(M_f^0 - M_f)}{A\rho_s} \quad (39)$$

where  $M_f^0$  is the mass of foam when the available volume is filled with dye water,  $M_f$  is the mass of empty foam only, and  $A$  is the total surface area of foam sample.

The foam was cut open and the depth that the dye water penetrated was measured. The penetration depth of dye water was 0.25 mm in a week, which was much smaller than

the dimensions of the foam sample (2.5\*2.5\*2.5 cm). In repeated experiments, data was shown reproducible (refer to lower curve in Fig. 12). This result showed the closed-cell structure of polystyrene foam.

Further tests for permeability of foam were also performed. When a surfactant was added to the dyed water (a few drops of liquid soap in ~ 500 ml water), the penetration depth doubled (Fig. 12). This result demonstrates the fact that adding a surfactant helps to wet the foam surfaces, because it increases the surface tension.

There was also a difference in the penetration of treated foams and untreated foams. Treated foams had been subjected to either an external applied pressure of from 1 to 5 atm or to a vacuum (refer to section III.B. 2 for further details). These pressure treatments may have damaged or broken the cell wall, thereby increasing the available volume. When the imbibition method was applied to treated foams [especially the one prepared under the highest pressure (5 atm)], the penetration depth was found to be about twice that of an untreated foam. The plots of penetration depth versus time elapsed for foams treated by low applied pressures were similar to each other (Fig. 13).

The penetration depth approached a saturation limit  $T_s$  (Fig. 13) at long times. We postulate this was related to the available volume becoming filled with imbibing liquid. The saturation depth, defined as  $T_s$ , is plotted versus applied pressure in Fig. 14. The increase in saturation volume with applied pressure differential confirms that damage was done to some cell walls, thereby increasing the available volume.

The penetration depth as a function of time can be related to the permeability of a material. Bear and Irmay show<sup>27</sup> the depth of the penetration front  $\zeta(t)$  of a fluid through a porous medium in time  $t$  is given by

$$\left(\frac{\rho g}{\mu n_e}\right) kt = \zeta - \left(H_0 + \frac{P_c}{\rho g}\right) \ln \left(1 + \frac{\zeta}{\left(H_0 + \frac{P_c}{\rho g}\right)}\right) \quad (40)$$

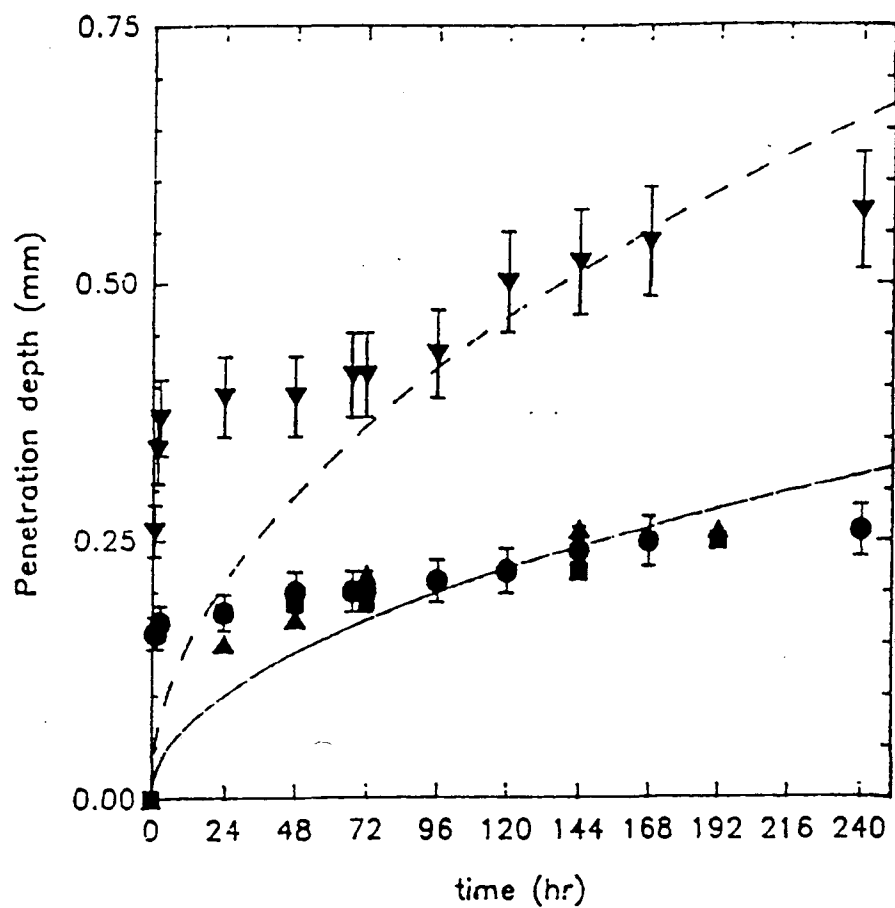


FIG. 12. Imbibition method: Comparison of penetration depth of foams with and without surfactant. Note that results for three different untreated samples of significantly different size and shape using an imbibing liquid without a surfactant are shown as solid circles, squares, and upward triangles. Data with a surfactant are shown as inverted triangles. The curves are based on fits to the data using Eq. 40.

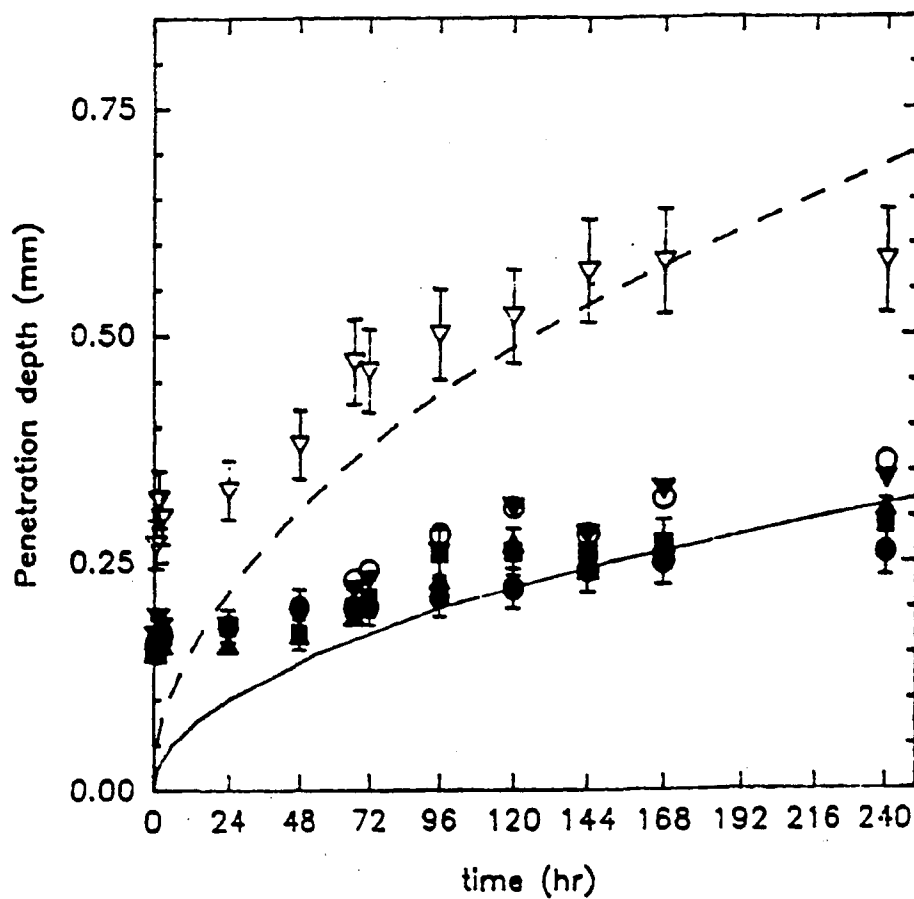


FIG. 13. Imbibition method: Comparison of different pressure differentials (solid circles, inverted triangles, squares, upward triangles, empty circles and inverted triangles stand for -1 atm, 0 atm, 1 atm, 2 atm, 3 atm, and 5 atm, respectively). The curves are for the untreated samples and the sample treated with a 5 atm pressure differential based on fits using Eq. 40.

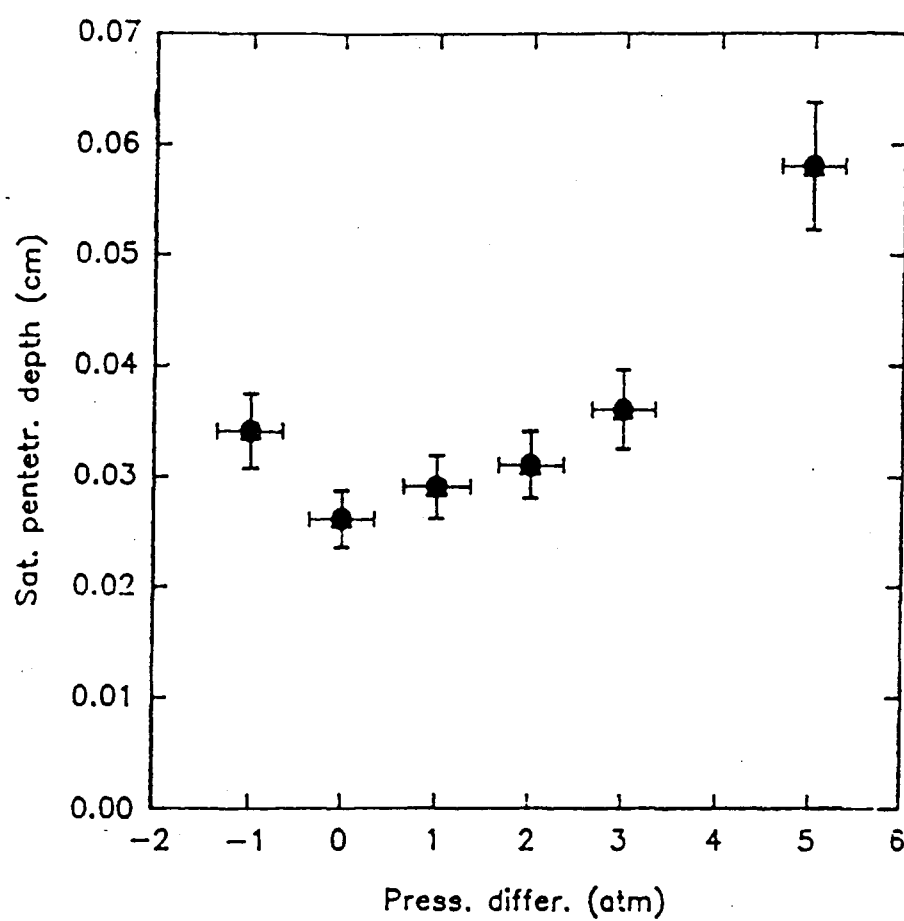


FIG. 14. Imbibition method: saturation penetration depth versus pressure differentials. Closed symbols are for measurements without a surfactant. The open symbol is for an untreated sample using a surfactant.

where  $\rho$  is the fluid density ( $10^3 \text{ kg m}^{-3}$  for water),  $g$  is the acceleration of gravity,  $\mu$  is the viscosity ( $1.002 \cdot 10^{-3} \text{ kg m}^{-1} \text{ s}^{-1}$  for water at 20 degrees C),  $n_e$  is the effective or available porosity of the medium (0.023 from Table 3),  $H_0$  is the depth of the fluid above the sample (approximately 2 cm),  $P_c$  is the ambient room pressure (approximately 0.8 atm or 8240 mm H<sub>2</sub>O), and  $k$  is the permeability. This assumes that  $H_0$  is constant, the penetration front is a step function with the partial pressure of the fluid changing from zero to  $P_c$  abruptly, that there are no effects of wetting, and that the available permeability is homogeneous throughout the sample.

The last two assumptions are known to present problems in our case. The doubling of the penetration depth with the addition of a surfactant indicates that wetting does occur. It would have been better to use a non-wetting fluid such as mercury, which is commonly employed in permeability and porosity tests. However, this effect should not have a large effect on the relative changes in permeability as a function of treatment with pressure differential. We expect the permeability to decrease with penetration depth as cell wall damage is reduced. Thus we would expect the above model to overestimate  $\zeta$  at large times.

The predictions of Eq. 40 for the untreated foam with and without surfactant are shown in Fig. 12; the permeabilities were determined to be  $(1.6 \pm 0.6) \cdot 10^{-19} \text{ cm}^2$  and  $(7.2 \pm 2) \cdot 10^{-19} \text{ cm}^2$ , respectively. The predictions of Eq. 40 for the untreated foam and the foam treated with a 5 atm pressure differential are shown in Fig. 13; the permeability of the treated foam was found to be  $(7.8 \pm 3) \cdot 10^{-19} \text{ cm}^2$ . For comparison, the permeabilities for clean gravel range from  $10^{-3}$  to  $10^{-5} \text{ cm}^2$ , for clean sand from  $10^{-5}$  to  $10^{-9} \text{ cm}^2$ , for clay from  $10^{-9}$  to  $10^{-16} \text{ cm}^2$ , and for rocks from  $10^{-7}$  to  $10^{-16} \text{ cm}^2$ . A plot of permeability as a function of applied pressure differential is shown in Fig. 15. This graph again demonstrates an increase in structural damage with applied pressure differential.

The BET method was described in the section on surface area measurements.<sup>26</sup> The

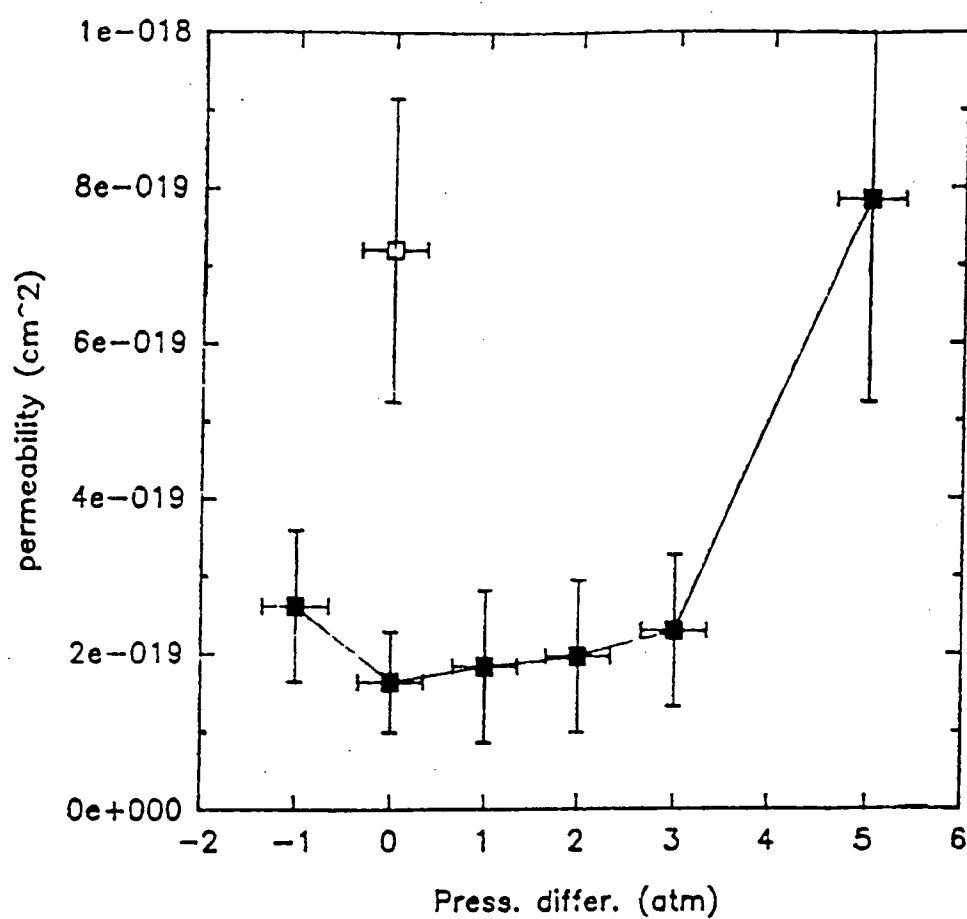


FIG. 15. Permeability versus pressure differential using imbibition method (solid squares stand for samples without surfactant.)

specific available surface area was found to be  $5.4 \text{ m}^2/\text{g}$  using the BET method.<sup>28</sup> Darcy determined the permeability by an equation (Eq. 5), which related the available porosity, available surface area, and permeability. The permeability for our untreated foam samples was calculated to be  $(3 \pm 0.5) \times 10^{-6} \text{ m}^2$  using Kozeny's relation.<sup>3</sup> The uncertainty is that the relation of the surface area measured with the BET method and that used in Kozeny's relation makes this determination of permeability of limited use.

## B. Structural Studies

### 1. Cell wall structure

Cells are the basic mesoscopic structural unit of foam. Many properties, including most mechanical properties, depend on the size, shape, and distribution of sizes of these cells and on the thickness and geometry of the cell walls. Thus, it is important to measure the cell size distribution and cell wall thickness distribution when characterizing foams. The cell size distribution and cell wall thickness distribution were measured to help understand the strength of cell walls and the transport properties. The methods used in this research to measure the distributions were the microscopy and photography methods.

The most direct method was to photograph a section of foam with a microscope and measure the cell size and wall thickness (see Fig. 16). A similar method was to photograph a block of foam with a macroscopic lens and to magnify the prints of observed foam cells (see Fig. 17). The cell structure was observed nonuniform, but similar to a hexagon. Both cell size distributions and cell wall dimensions were fit with Gaussian distributions. The average cell radius was  $1.1 \pm 0.3 \text{ mm}$  (see Fig. 18). The cell radius distribution had a FWHM of  $0.78 \pm 0.04 \text{ mm}$ . The average cell wall thickness was  $0.04 \pm 0.01 \text{ mm}$ , which was about one thirtieth of the size of a cell (Fig. 19). The cell wall thickness distribution had a FWHM of  $0.029 \pm 0.002 \text{ mm}$ .

Base on the average dimensions, the relative density was estimated to be

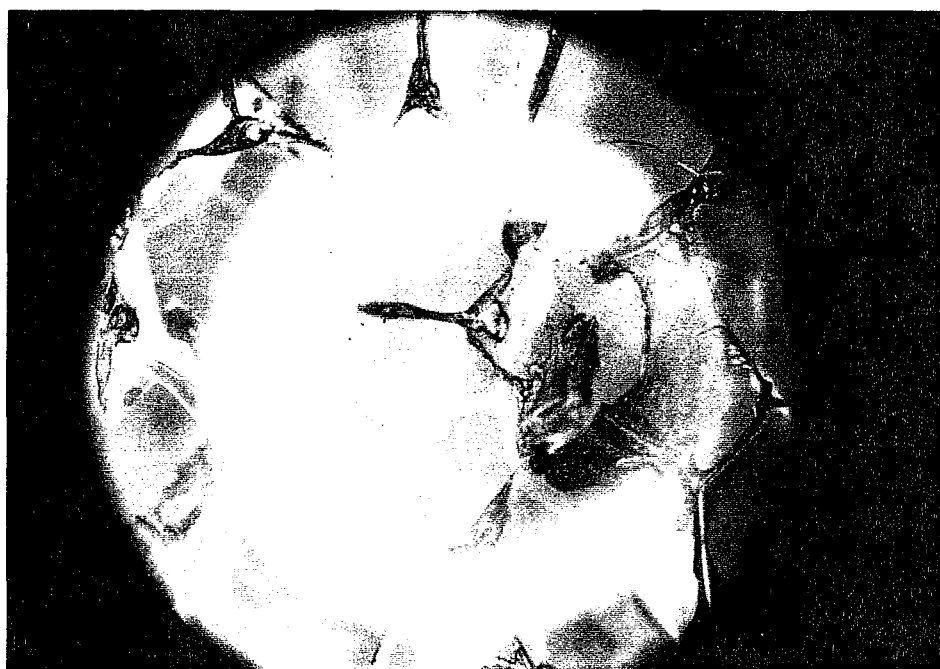


FIG. 16. Micrograph of polystyrene foam.

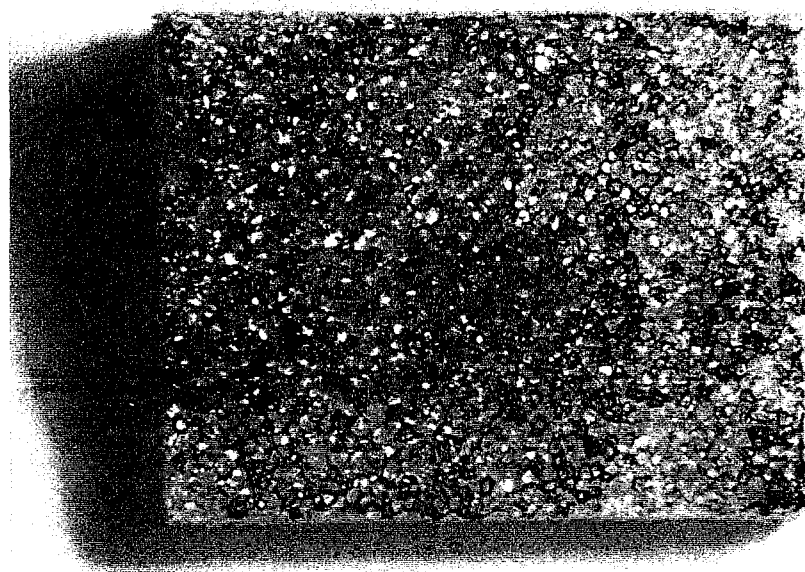


FIG. 17. Photograph of polystyrene foam. The cell structure has been highlighted by coloring the foam surface.

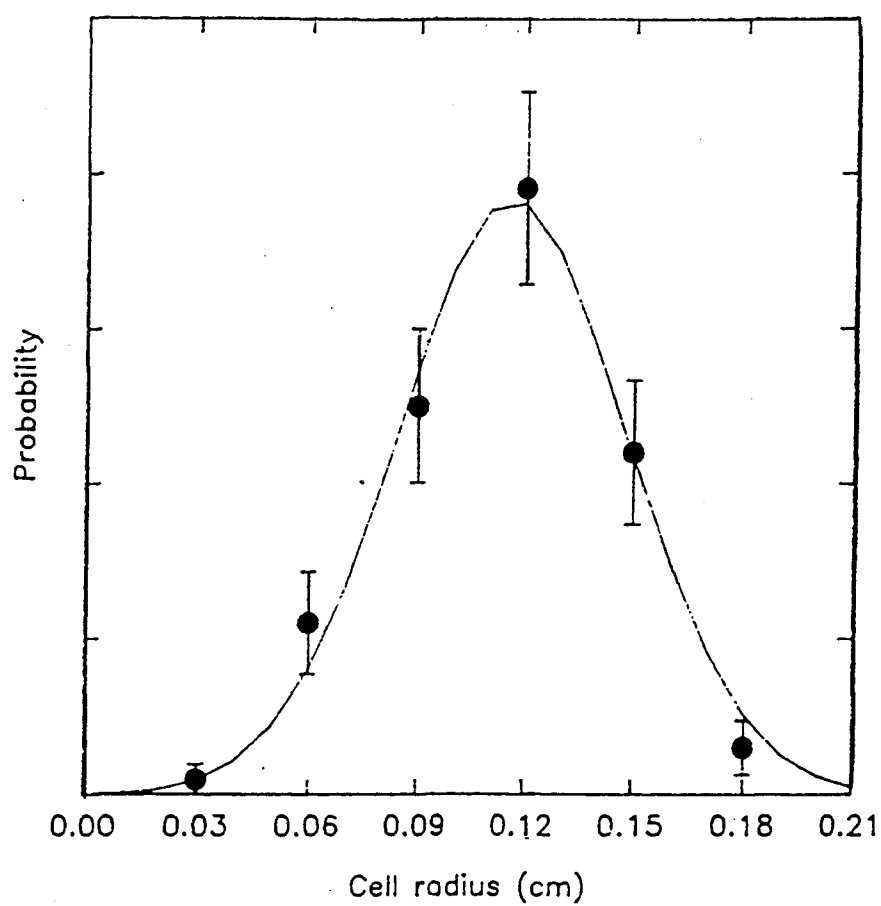


FIG. 18. Cell size distributions of polystyrene foam.

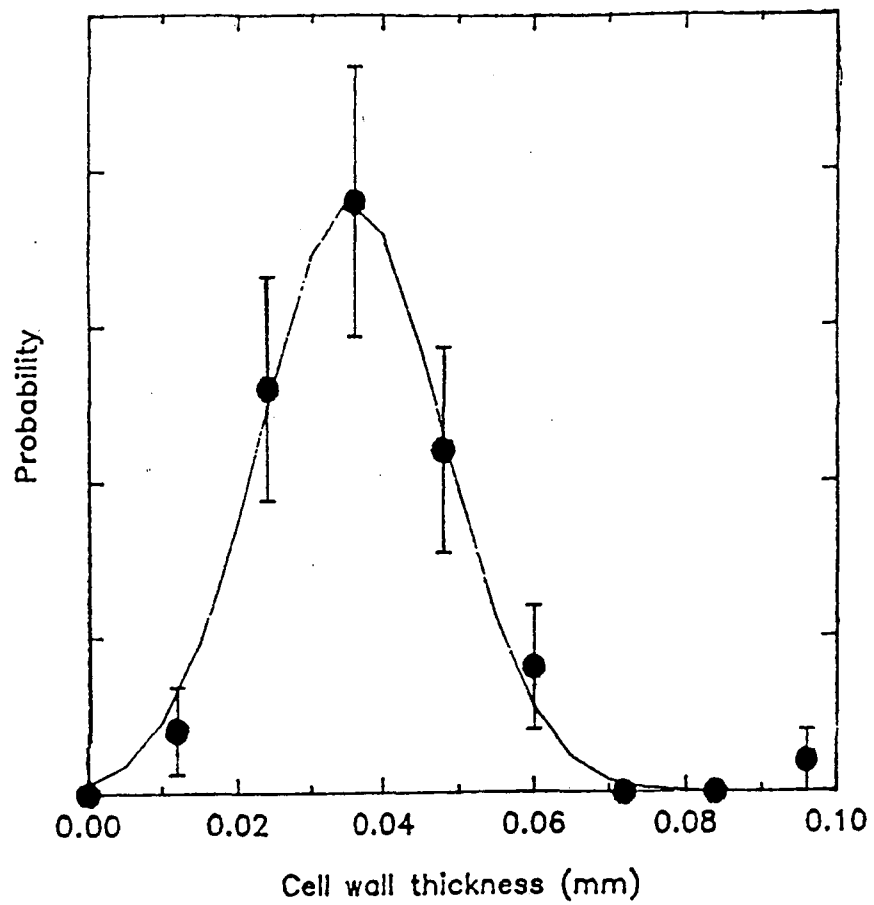


FIG. 19. Cell wall thickness distribution.

$0.06 \pm 0.03$ , using the method described in section III.A.2. This is 70% greater than the accepted value, suggesting that either the measured thickness was in serious error or that the cell walls were not of uniform thickness and large portions were thinner than our measurement indicated. The latter is consistent with the idea that the beams were thicker than the central portions of the wall due to surface tension effects during wall formation.

Alternate methods to measure these distributions include small angle x-ray scattering, light scattering, adsorption isotherms, and ultrasonic methods. These experiments were not accomplished in the limited time. However, the light scattering method for studying the foam structure will be discussed in details later in the section on density gradients (section III. C.). A brief discussion of the small angle scattering method, of adsorption isotherms, and ultrasonic method were given in section II.

## 2. Pressure box tests

A series of measurements was designed to study structural properties of foam samples subjected to an external pressure or vacuum. Each sample was held at the applied pressure for  $\sim 24$  hours. The major apparatus used was a pressure box (Fig. 9). We hypothesized that cell wall damage induced by the pressure treatment would have a significant effect on the mechanical properties of the foam. Damage from cell wall buckling or rupture of the thin central part of the cell wall may be caused by a pressure differential between the interior and the exterior of the cell. The external applied pressure varied from vacuum to  $\sim 5$  atm. We estimate the pressure inside the cell walls as  $1 \pm 0.5$  atm. The equilibrium vapor pressure of the solvents used in the foaming process at room temperature is typically 0.5 to 1 atm. The foaming process is done with the resin at elevated pressures, so it is not unreasonable to expect the initial trapped gas to be above 1 atm. Outgassing measurements (see section V. D.) suggest that the cell walls allow slow gas diffusion (on the order of hours or days) and that the cells were at approximately 1 atm.

The pressure box inside dimensions are  $10 \times 15 \times 3.85 \text{ cm}^3$ , with a volume of  $577 \pm 25 \text{ cm}^3$ . It was equipped (refer to Fig. 9-11) with a gas inlet port, a vacuum port, a ballast volume, pressure gauges (including an ion gauge, a vacuum thermocouple gauge, Si manometers, and Bourdon gauges), temperature gauges, and a temperature controller (using a  $50 \text{ } \Omega$  resistance heater, monitored by thermocouple and RTDs, and controlled to within 1 K). This box was designed to operate in a pressure range of micro torrs to 10 atm, and in the temperature range of -23 to 177 degrees C. The system was interfaced to a computer with an ADC board for automated data collection. The vacuum system used a mechanical pump and a diffusion pump with an ultimate pressure of  $10^{-6}$  torr.

The gas expansion method was applied to study the structure of polystyrene foams, which included five steps:

a. We calibrated the system volume, which included the pressure box and the fittings. The pressure box was connected to the gas handling system (GHS), which was equipped with a large and a small standard volumes. The large standard volume was  $292.03 \text{ cm}^3$ , the small standard volume was  $39.4 \text{ cm}^3$ , and the manifold volume was  $46.5 \text{ cm}^3$ . By expanding gas from  $V_0$  to  $V_1$

$$V_{1_n} = V_0 \times \left( \frac{P_{0_n}}{P_{1_n}} \right) \quad (41)$$

where  $V_1$  included the fill line and GHS volumes,  $V_0$  was the volume of GHS,  $P_0$  was the initial pressure of the GHS, and  $P_1$  was the expanded pressure of the GHS and the fill line to the pressure box.

Expanding further into  $V_2$ , we have

$$V_{2_n} = \left( \frac{P_{1_n} - P_{2_n}}{P_{2_n}} \right) \times \left( \frac{T_{pb} P_{2_n}}{T_{ghs} P_{1_n}} \right) \times V_{1_n} + V_{1_n} \quad (42)$$

where  $V_2$  includes  $V_1$  and the ballast volume on the pressure box;  $P_2$  is the expanded

pressure of the GHS, fill line, and the ballast volume;  $T_{pb2}$  is the temperature of the pressure box; and  $T_{ghs2}$  is the temperature of the GHS.

Finally, expanding into  $V3$  we have

$$V3_n = \left( \frac{P2_n - P3_n}{P3_n} \right) \times \left( \frac{T_{pb3_n}}{T_{ghs3_n}} \right) \times V2_n + V2_n \quad (43)$$

where  $V3$  includes  $V2$  and the pressure box;  $P3$  is the final pressure of the whole system with every valve open;  $T_{pb3}$  is the final temperature of the pressure box; and  $T_{ghs3}$  is the final temperature of the GHS.

Notice that the temperatures used here are in degrees Kelvin. The volume of the gas handling system (including the large standard volume, small standard volume, and all the valves) was measured as  $377.93 \text{ cm}^3$ . The measurements were repeated several times. The average volume of the fill line was  $9.206 \text{ cm}^3$ . The average volume of the ballast was  $435.457 \text{ cm}^3$ . The average volume of the pressure box was measured by this method as  $603.646 \text{ cm}^3$ .

b. One block of untreated foam (at ambient pressure) was placed in the pressure box at a time. The samples were initially of the same size.

c. Nitrogen gas was let into the system to predetermined high pressures. The initial pressure, the balanced pressure, and the temperature of the pressure box were recorded.

d. The ideal gas law was used to calculate the available volume from the final pressure of the gas in the pressure box. The relation between available volume and applied pressure can be found as follows

$$V_n^f = \left( \frac{P_n^i - P_n^f}{P_n^f - P_{atm}} \right) (V2 - V1) \quad (44)$$

assuming  $P_{atm} = 1 \text{ atm}$ , where  $P_i$  is the applied pressure,  $P_f$  is the final pressure; and  $V1$  and  $V2$  were defined in the calibration of pressure box. Note  $P^f$  and  $P^i$  are gauge pressures. By

knowing the exact inner volume of the pressure box and the foam volume, the available volume of foam can be calculated.

e. The estimated available volume versus pressure differential curve is plotted in Fig. 20.

Foam samples treated by different pressures were taken out of the pressure box and found to be curved (see Fig.21). This showed the nonuniformity of compression by applied pressure on the foams. The pictures showed that under high pressures, the cut surfaces contracted much more than the uncut surfaces. The higher the applied pressure, the smaller the curvatures, and the more the volume shrinkage (Table 4). The radii of curved top surfaces and bottom surfaces were measured. It was verified that the cut surfaces were the ones with smaller curvatures

A measure of the anisotropy of the strain in the cut and uncut surfaces is given by

$$Anisotropy = \frac{\delta l_c / l_c^0}{\delta l_u / l_u^0} = \frac{l_c - l_c^0}{l_u - l_u^0} \quad (45)$$

where  $l_c$  and  $l_u$  are the lengths of the cut and uncut surfaces after the applied pressure differential,  $l_c^0 = l_u^0$  is the initial length, and  $\delta l = l - l^0$ . A plot of anisotropy versus pressure differential is shown in Fig. 22.

### 3. Mechanical tests

To test the strength of foam samples and verify the applicability of Ashby's model (mentioned in the previous chapter) and to investigate the effects of the applied pressure differential, mechanical compression and deflection tests were done to test for strength decrease due to the applied pressure differential. The mechanical tests were done at the Thiokol Corporation laboratories.

a. Compression test. In the compression tests (see Fig. 23), six foam samples

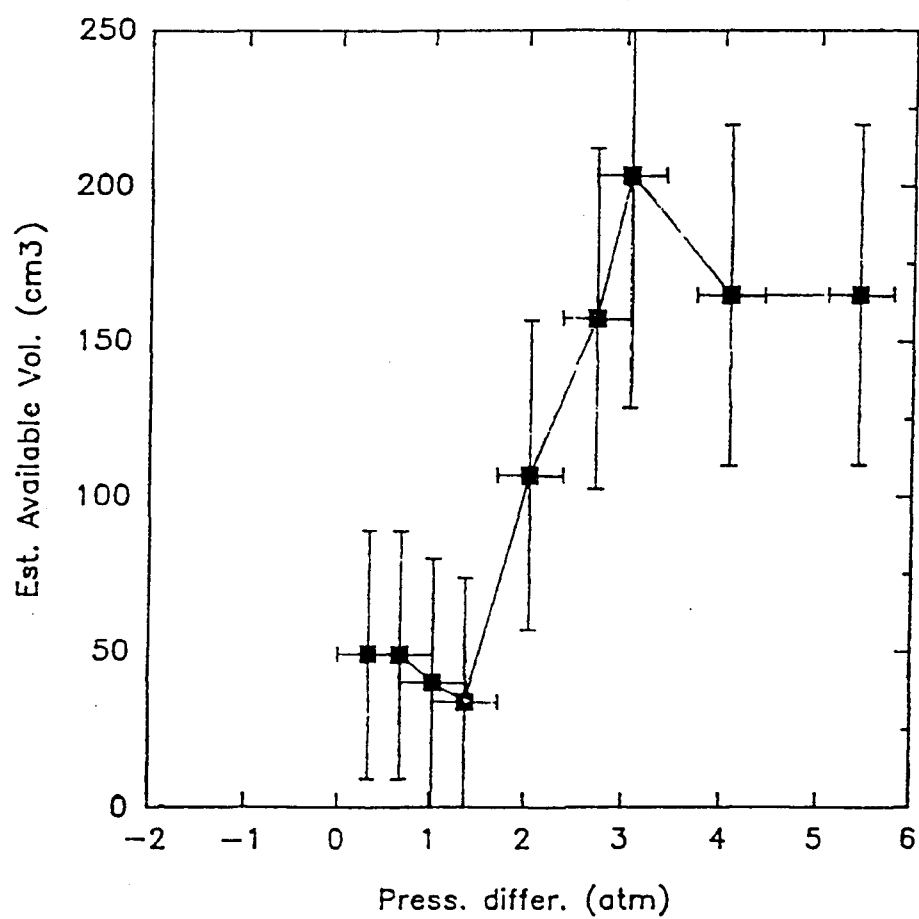


FIG. 20. Estimated available volume versus pressure differential.

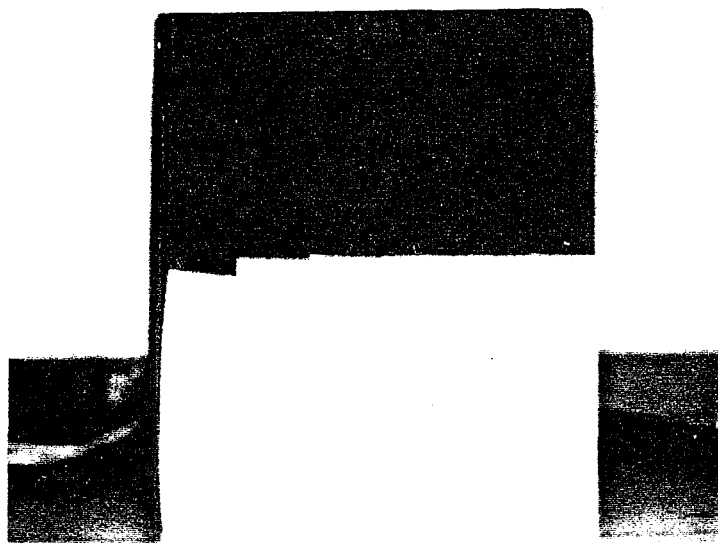


FIG. 21. Compression of six polystyrene foam samples treated with pressure differentials.

Table 4. Radii of the curved foam surfaces.

Pressure Differential (atm)	Cut surface displacement (radius) (mm)	Uncut surface displacement (radius) (mm)	Relative volume shrinkage (%)	Relative density	Strain anisotropy (colm1/ colm2)
-1	0.5 (625)	0.5 (625)	0	0.028	1.00
0	0.5 (625)	0.5 (625)	0	0.028	1.00
1	0.7 (447)	0.45 (695)	5	0.029	1.56
2	0.8 (391)	0.35 (893)	4	0.029	2.29
3	0.85 (368)	0.40 (782)	14	0.033	2.29
5	-----	-----	----	----	----

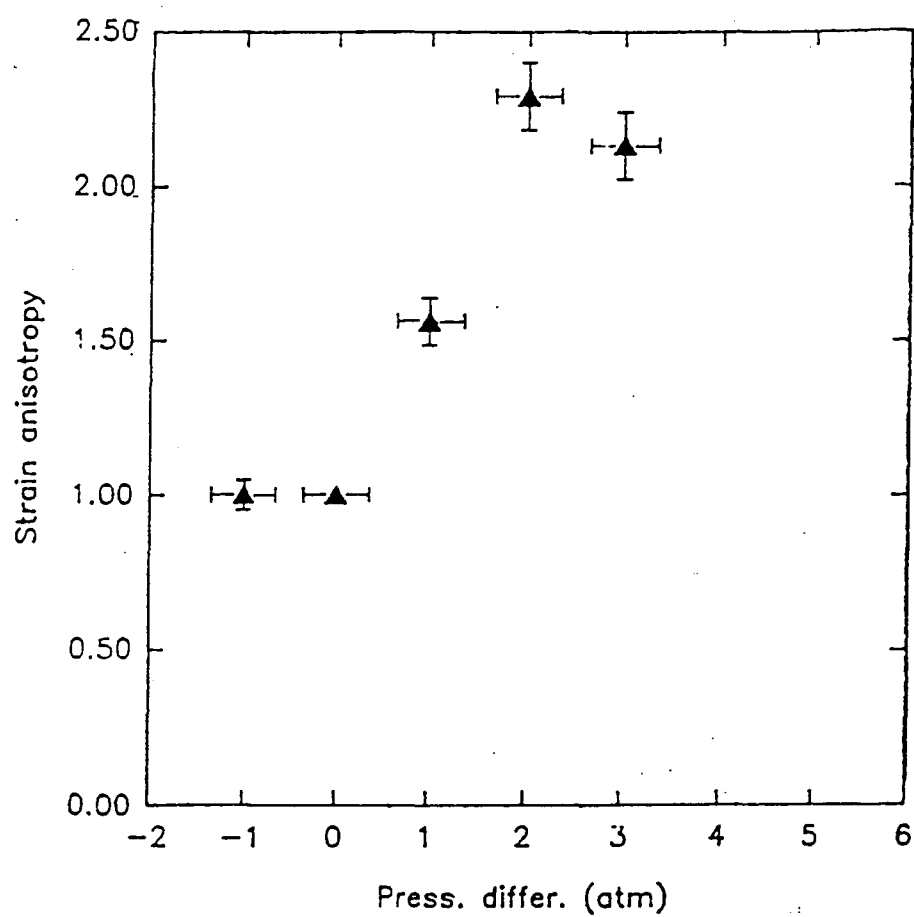


FIG. 22. Pressure box tests: Anisotropy versus pressure differential.

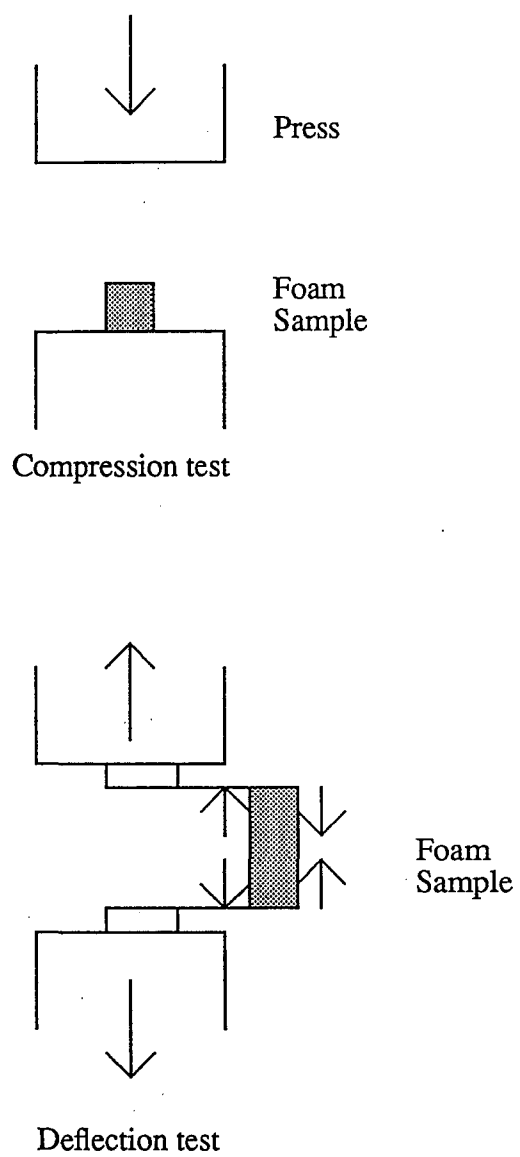


FIG. 23. Setup of compression and deflection tests.

treated under different pressures were tested, which were originally of identical height (5 cm). The samples were compressed by a constant rate of external forces. The maximum stresses were identical (4.1 MPa or 41 atm). The samples were compacted to almost identical maximum strains of  $\sim 0.9$ .

The stress-strain curves for compression of the treated samples (see Fig. 24) have three regions, which were consistent with the Ashby's model of cellular foams (see Fig. 5). If one compares the different curves, the elastic collapse stress  $\sigma_{pl}^{\circ}$  (maximum stress in the linear elastic region) decreases with increasing applied pressure (see Fig. 25). The linear elastic region and the plateau are much smaller for the samples treated with over 2 atm of pressure differential. The slope of the linear elastic part is the Young's modulus, which characterizes the strength of foam structures (Fig. 26). The Young's modulus decreases significantly above a pressure differential of 2 atm, indicating significant damage for larger pressure differentials. Table 5 lists the Young's modulus  $E$  and the reduced Young's modulus  $E/E_s$ , where  $E_s$  (2650 MPa) is the Young's modulus of bulk polystyrene,<sup>22</sup> Table 5 also lists the elastic collapse stress  $\sigma_{el}$  and the relative elastic collapse stress  $\sigma_{el}^*/E_s$ . The elastic collapse stress is the point at which elastic buckling of the cell walls begins, that is, the point where the compression stress-strain curves (Fig. 20) deviate from the initial linear elastic behavior. This is plotted versus applied pressure differential in Fig. 27.

It is common for samples to bulge in the middle, producing barrel-shaped distortions during compression tests. During our compression procedures, the foams distorted in different directions depending on the applied pressure differential. Sample one was treated under vacuum; it distorted in the typical barrel fashion. Here, the pressure of the voids inside the foam was higher than the applied vacuum outside the foam, which would cause the cell walls to buckle outward. Differently, sample two was treated with no pressure differential; it did not distort apparently in any direction during the compression test. Here, the pressure inside the voids was the same as outside. By contrast, the outer cell

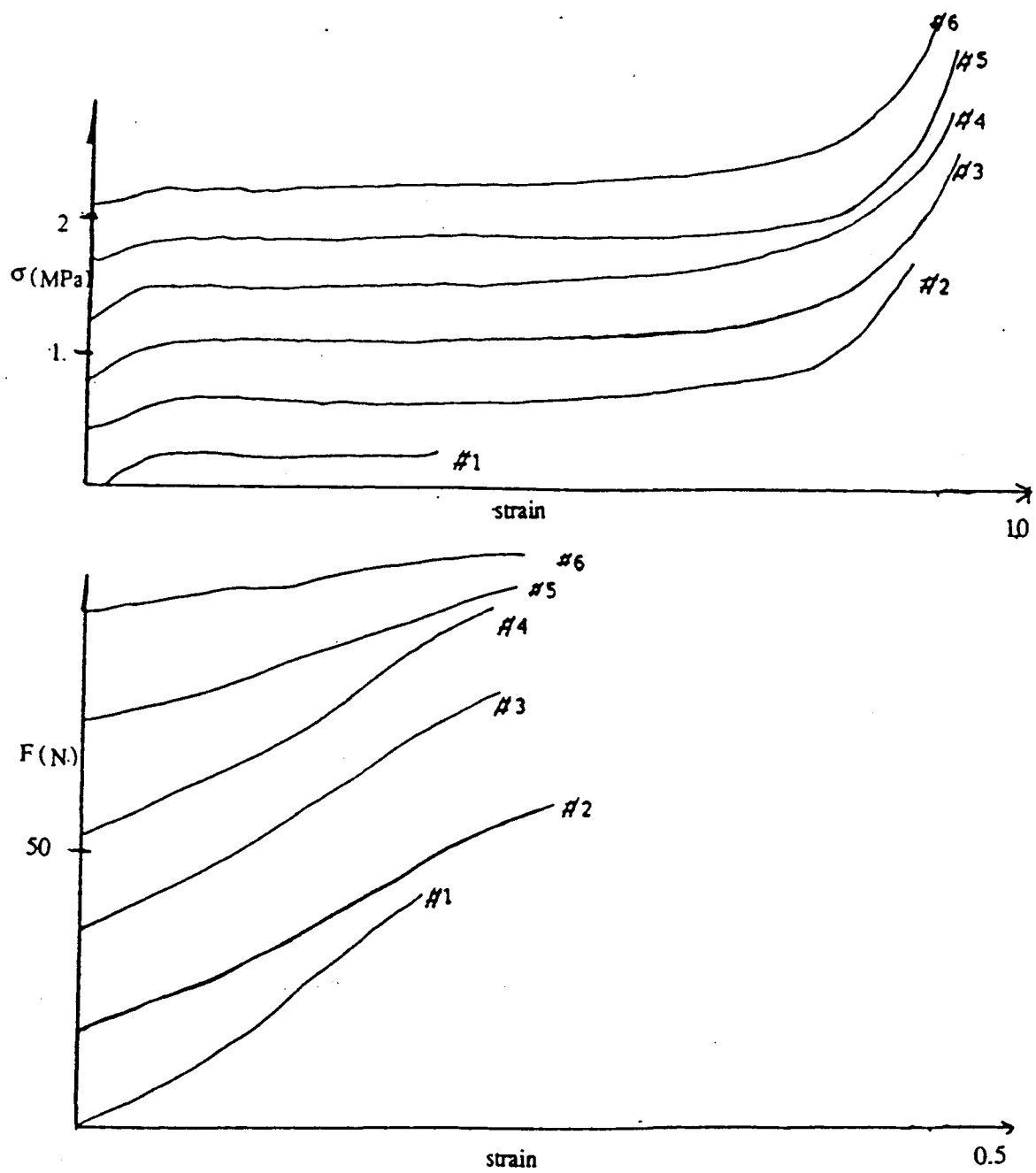


FIG. 24. Stress versus strain of compression (top) and deflection (bottom) tests. Note zeros are shifted for each curve.

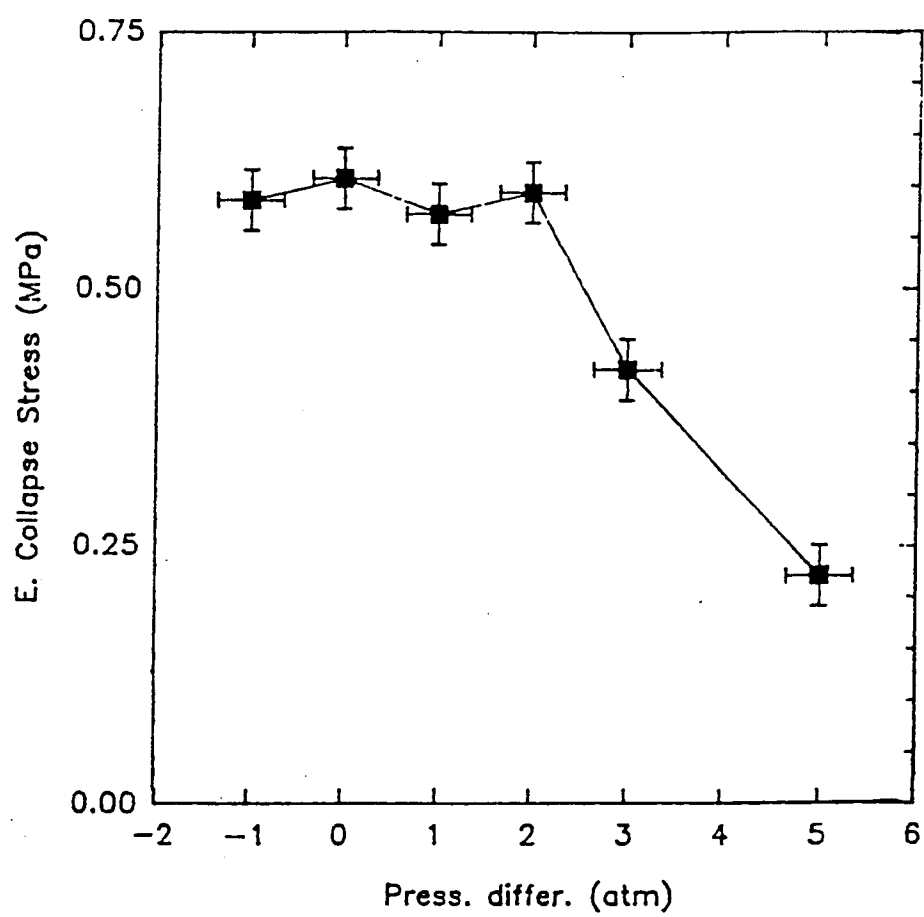


FIG. 25. Compression test: Elastic collapse stress versus pressure differential.

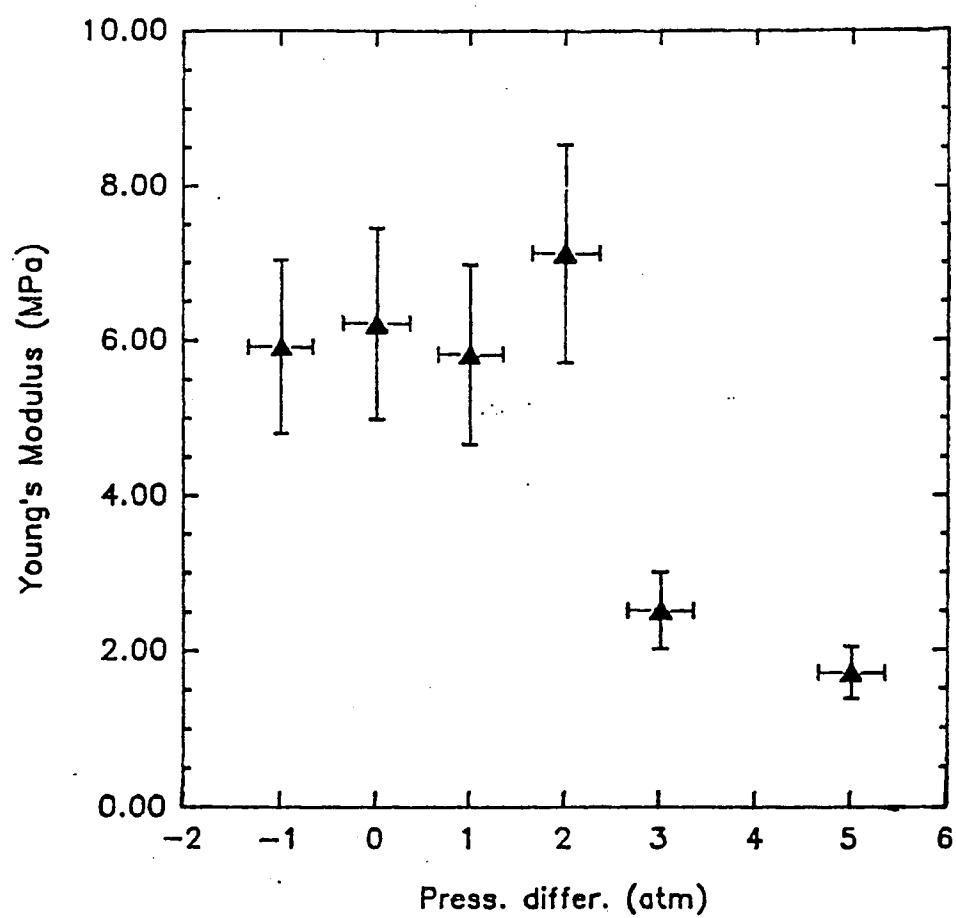


FIG. 26. Young's modulus versus pressure differential.

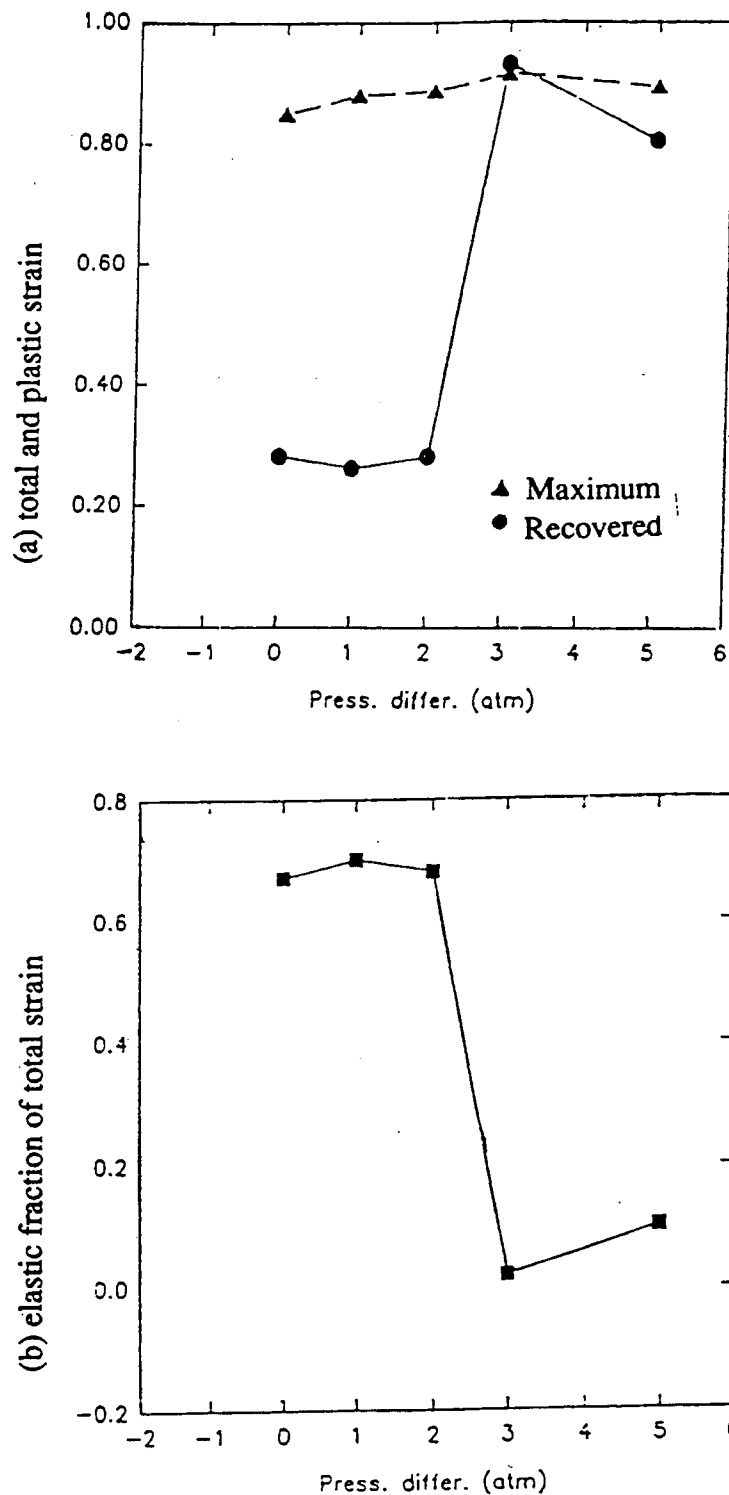


FIG. 27. Compression test: (a) The total strain under maximum applied loads ( $\sim 4.1$  MPa) is shown with solid triangles and the plastic strain still present after full recovery is shown with solid circles, (b) the elastic fraction of total strain versus pressure differentials.

Table 5. (a) Compression and (b) deflection tests of polystyrene foams. Note that  $\rho_s$  is 1.05 g/cm<sup>3</sup> (Table 2),  $E_s$  is 2650 MPa (Ref. 23).

Pressure differential (atm)	Original height (cm)	Maximum compressions (max. strain) (cm)	Relative Density	Elastic Collapse Stress (MPa)	Relative Elastic Collapse Stress	Young's Modulus (MPa)	Relative Young's Modulus
-1	5.01	2.77 (55.3%)	0.031	0.59	0.00022	5.9	0.0023
0	5.22	4.43 (84.9%)	0.028	0.61	0.00023	6.2	0.0023
1	5.20	4.57 (87.9%)	0.029	0.57	0.00022	5.8	0.0022
2	5.24	4.54 (86.6%)	0.028	0.59	0.00022	7.1	0.0028
3	4.99	4.56 (91.4%)	0.032	0.42	0.00016	2.5	0.0009
5	4.89	4.43 (89.0%)	0.034	0.22	0.00008	1.7	0.0006

Pressure differential (atm)	Ultimate Tensile strength (kPa)	Maximum Displacement (cm)
-1	26.3	0.91
0	25.6	1.24
1	26.4	1.09
2	26.5	1.14
3	18.5	1.45
5	10.6	2.21

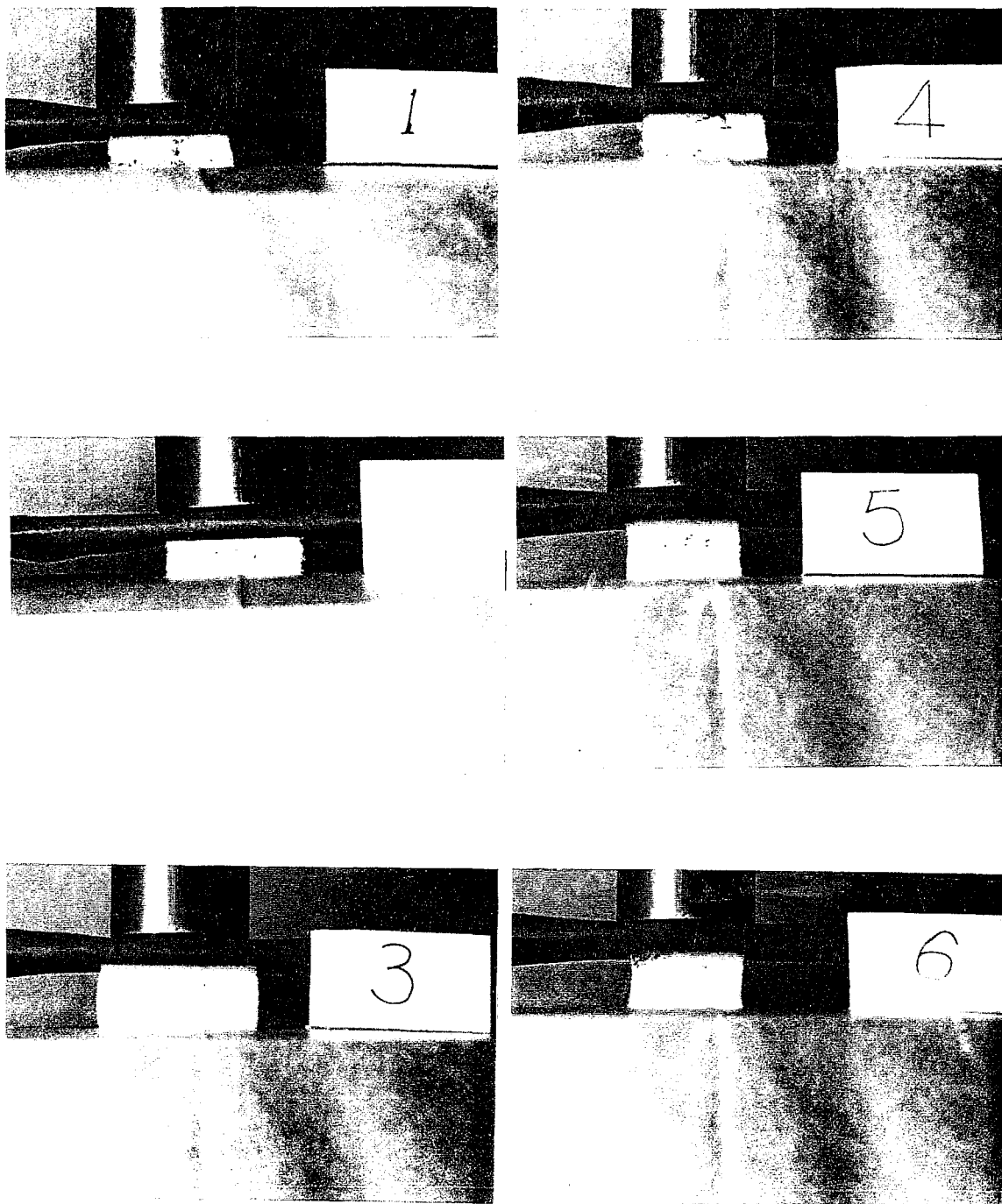


FIG. 28. Photographs of barrel-shaped distortions of polystyrene foams.



FIG. 29. Micrographs of six compressed polystyrene foam samples treated with pressure differentials from -1 to 5 atm. Micrographs from top to bottom and left to right have applied pressure differentials of -1 atm, 0 atm, 1 atm, 2 atm, 3 atm, and 5 atm, respectively.

walls were buckled inward when they were under high pressure differentials. Samples numbered three to six all showed inverted (concave) barrel-shaped distortions during the compression tests (Fig. 28). Micrographs of treated samples (see Fig. 29) showed cell walls buckled outward when a vacuum was applied. Increasing inward buckling and eventual cell wall rupture were observed in micrographs of samples treated with applied pressures of up to 5 atm.

Another phenomenon was that the foam samples did not recover elastically to their initial sizes even after the applied pressure was removed. Each treated sample was subjected to a maximum load of 4.1 MPa (for only a few minutes) during the compression test, which resulted in strains of ~90% for all samples (see Fig. 22 and Table 5). After several days the samples had recovered some or most of their initial height. This recovery was due to the elastic resilience of the foam via an anelastic response. Figure 27 (a) shows the strain (elastic plus plastic strain)  $\delta l_{max}/l_0$  at maximum applied stress and the strain after recovery (plastic strain only)  $(\delta l_{recovered})/l_0$  as a function of applied pressure differential. The difference of the maximum strain and recovered strain divided by the maximum stress is a measure of the fraction of the elastic strain component of the maximum strain [see Fig. 27 (b)].

Note the amount of plastic deformation is much greater for sample treated with pressure differentials in excess of 2 atm (0.2 MPa). It is important to realize that much higher stresses applied for a short time during the compression test do not cause extensive plastic deformation; it is only stresses above 2 atm applied for long periods of time that cause such deformation.

b. Deflection tests. In the deflection tests (see Fig. 22) one side of the foam sample was pulled and rotated at the same time. Therefore, the inner side is under tension, while the outer side is under compression. The external applied force was multiaxial. The

maximum angle of deflection is

$$\theta(x) = \frac{1}{EI} \int M(x) dx \quad (46)$$

where  $x$  is the displacement along the length  $L$  of the sample,  $M$  is the internal moment, and  $I$  is the moment of inertial. Apply the boundary condition  $d=0$  at  $x=0$ . Therefore, at the center line ( $x=L/2$ ), the Young's modulus is

$$E = \frac{ML^2}{8I\delta_c} \quad (47)$$

where the deflection is

$$\delta(x) = \int \theta(x) dx \quad (48)$$

Samples were broken when the maximum tolerance of force was reached (Table 5). The stress-strain diagrams were linear (with small oscillations). The slopes of the plots decreased as the applied pressure increased. The ultimate strength of foam samples decreased dramatically, when the pressure differential of the foam exceeded 2 atm (Fig. 30). In the microscopic pictures of the broken cross sections of the foams, the homogeneous deformation of cell walls are shown (see Fig. 29).

### C. Density Gradients

In order to study the macroscopic and small scale density variations and the structural integrity of foams, a series of simple optical measurements was designed. These experiments are based on the measurements of the transmission, reflection, and scattering of the visible light by polystyrene foam samples.

The optical transmission method was used to study the density gradients and the

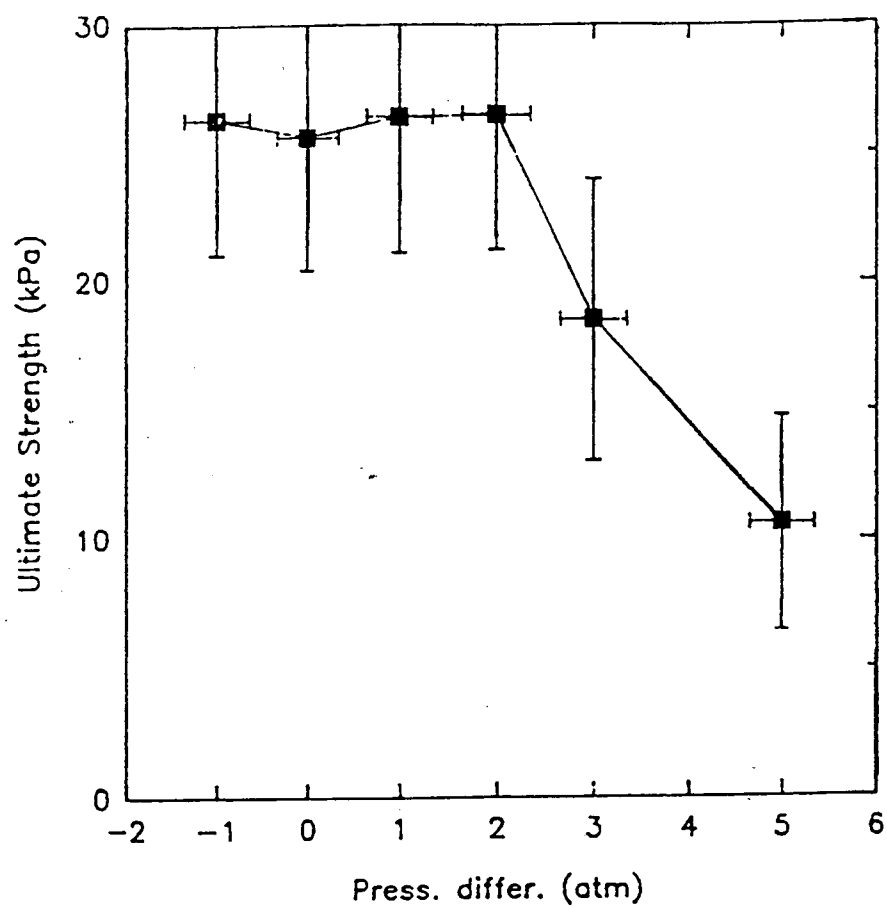


FIG. 30. Deflection test: Ultimate strength versus pressure differential.

inhomogeneity of foams. The sets of experiments performed used photographic and laser transmission methods.

### 1. Photographic method

The photographic method is a direct way to show the density gradient of the polystyrene foams. A foam sample placed on a film was exposed for a long period of time under controlled light and then developed. This method was also applied to the Thiokol strut samples. Density variations of both the commercial polystyrene foams and the Thiokol strut samples were studied.

### 2. Laser transmission method

The purpose of this set of experiments was to use laser light transmission to map the density of polystyrene foam (both commercial and the Thiokol foams). The experimental apparatus is shown in Fig. 31. The light source is a 1 mW HeNe laser at 633 nm wavelength. An optional beam expander is used to produce large radius columnated beams ( $\sim 0.5$  to 5 cm diameter). An adjustable diaphragm limits stray light and the size of the expanded beam. An alignment screen is used to assure normal incidence on the sample. An optional lens is placed in front of the detector to focus the transmitted light into the detector. A collimating light shield and a detector aperture limit the light incident on the photocell detector. The Meteorologic 45-540 photometer has a dynamic range of  $10^6$  from 30 nW to 30 mW. An analog output from the photometer is fed into a computer via an A/D interface board. Data collection is triggered by the keyboard.

More details of designed optical measurements of foam will be placed in the proposed future work section.

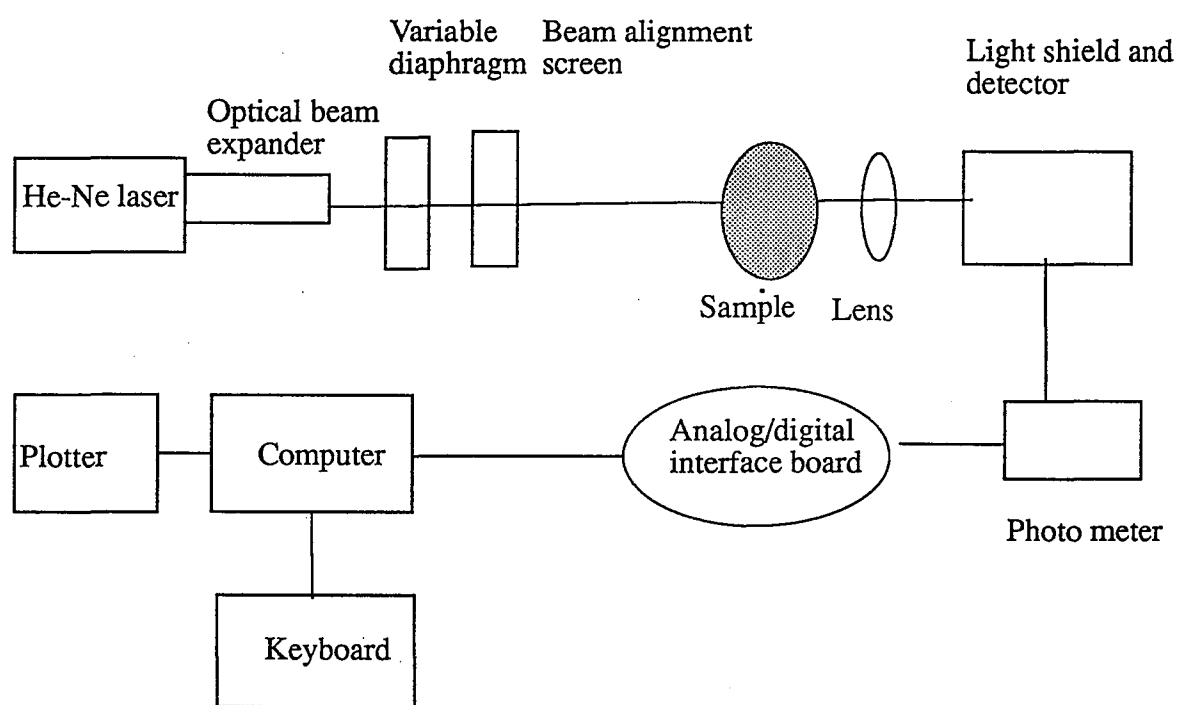


FIG. 31. Block diagram of apparatus for optical measurements of foams.

#### IV. ANALYSIS OF RESULTS

In this section, applied experimental methods are evaluated and the results are presented and analyzed. These analyses have the goal of determining the requirements for material selection of lightweight and strong materials.

##### A. Summary of Foam Characteristics

Originally, the commercial polystyrene foam is nearly isotropic: therefore, its structure and properties have no directionality. It is characterized by closed cells of a roughly uniform size. However, it is believed that surface tension draws much of the solid material into the cell edges during manufacture, thus the closed-cell faces behave structurally like faces of open-cell foams. Also, during material preparation and the tests performed, foam surfaces were either cut or pressed by different methods. These external forces change the foam cells to become anisotropic, which can also be characterized by open-cell models.

Among the chosen experimental methods for studying density, the gravimetric method gives the best result of bulk polystyrene density. Compression test yields the highest uncertainty because of the uncertainty of the bulk volume measurement. Both Archimedes' method and the gravimetric method give results close to the tabulated density of polystyrene foam. The density of polystyrene bulk is about 30 times the density of foam. This result matched the ratio of cell size and cell wall dimension, which will be mentioned later. Based only on density considerations, foams fit the requirement of being a lightweight material.

All the methods used for measuring total porosity lead to high values in excess of 90%; therefore, foam was shown to be a highly porous material. Of these methods, the pressure-volume curve gives the result with smallest uncertainty. The microscopy method yields the highest uncertainty, which comes from the uncertainty of cell size distribution and cell wall dimension. The average total porosity showed that most of the foam volume

was composed of voids. The average available porosity was much smaller than the total porosity, which showed that only a few voids near the sample surface were open to the environment. Imbibition method was found a better method for studying available porosity than the Archimedes' method. However, the Archimedes' method can be improved by an accurate measurement of foam volume.

The low permeability ( $3 \times 10^{-6} \text{ m}^2$ ) reflected the small available porosity, and proved the cell structure of polystyrene foam was essentially closed. The author found that it was easier to wet the foam surfaces by adding a surfactant to the imbibing water. The amount of water with a surfactant trapped in available volume was about twice the amount without surfactant. By repeating the experiment, this result of imbibition method was proved reproducible.

Only the BET method was used to study surface area; a large available surface area was obtained.

Microscopic examination of foam samples found that both the cell size distribution and cell wall thickness distribution were Gaussian. The average cell size is approximately 30 times of the average cell wall dimension.

## B. Mechanical Properties

The mechanical properties of commercial polystyrene foam samples were studied using a standard compression test and a deflection test. In general, all our results were consistent with those reported by previous investigators and were modeled well by the theories of Ashby and others reviewed in section II. B. The stress-strain curve for the untreated foam exhibited the three regions of linear elastic deformation, plastic plateau of deformation, and densification predicted by Ashby. Our measured values of relative Young's modulus, relative elastic stress, collapse stress, and densification strain limit were all in the expected range. The deflection test exhibited an ultimodulusmate stress in the expected range. In summary, we can say that the mechanical properties of the untreated

foam samples had values in the expected range, were well understood based on theoretical models, and were acceptable for our proposed application as materials for struts for innovative space structures.

### C. Effects of Applied Hydrostatic Pressure

A series of experiments was performed to study the foam characteristics, mesoscopic structure, and mechanical properties of foams when they were subjected to a modest hydrostatic pressure differential for a long period of time on the order of 24 hours. We hypothesized that cell wall damage induced by the applied pressure differential would have a significant effect on these foam properties. The effects of such an applied pressure differential are of particular importance to our applications in space, since we expect that there may be a similar pressure differential between the interior of the foam cells and the space vacuum environment during deployment and curing of the struts.

Significant effects in almost all properties tested were observed when the pressure differential exceeded 2 atm. There were indications that effects still existed at more moderate pressure differentials. Changes in properties at modest pressure differentials, particularly mechanical properties, such as Young's modulus, relative elastic collapse stress, and ultimate strength, can have crucial determinantal effects on our proposed applications and must be examined carefully. The changes in macroscopic properties due to applied pressure differential were consistent with changes observed in mesoscopic structure of the treated foam samples and foam cells. The importance of long-term exposure to hydrostatic pressures was also demonstrated; application of much higher uniaxial stresses (up to twenty-five times the 2 atm threshold) for short periods of time did not produce the same effects. We will now review the changes observed due to applied pressure differential.

The permeability (Fig.10), penetration depth (Figs. 13 and 14), and available volume (Fig. 19) all showed a continuous change with increasing applied pressure

differential, with a maximum change of more than a factor of two. It should be noted that these properties also showed a similar change when a negative pressure differential (vacuum) was applied. These results can be understood as the result of structural damage in a thin region near the surface of the foam samples due to cell wall buckling or rupture of the thin central part of the cell wall. Micrographs of treated foams (Fig. 29) confirmed this type of cell wall damage occurred.

Stress-strain diagrams of compression tests of the treated foam samples (Fig. 23) also showed pronounced differences for both positive and negative pressure differentials. Above 2 atm applied pressure differential, both the Young's modulus (Fig. 25) and the elastic collapse stress (Fig. 24) showed pronounced decreases. At 5 atm pressure differential, both these crucial properties decreased by approximately a factor of three. Foams treated with applied pressure differential not exceeding 2 atm were found to have a fairly high resilience, recovering approximately 75% from short-term uniaxial compressive stresses in excess of 40 atm (see Fig. 27). Samples subjected to higher applied pressure differentials showed virtually no resilience. This implies that most of the deformation due to the applied pressure differentials up to 2 atm was elastic, while above this applied pressure differential the deformation was plastic.

Mechanical deflection tests also showed the effects of the applied pressure differential. This was a more complicated test than the compression test and it exerted stress along all three axes. The ultimate strength in deflections reduced significantly above applied pressure differentials of 2 atm and decreased by a factor of 2.5 at 5 atm applied pressure differential. The elastic modulus [as reflected in the slope of the deflection test stress-strain curves (Fig. 23)] also showed a similar trend.

An interesting macroscopic effect was observed while the treated foams were under maximum compression testing. While the untreated sample did not exhibit any appreciable barreling (i.e. had a very small Poisson's ratio), the treated foams behaved differently (Fig.

26). The foam sample subjected to a vacuum exhibited significant barreling with a positive Poisson's ratio. Most samples treated with a positive pressure differential, however, had an hourglass shape, exhibiting a negative Poisson's ratio. The effect was more pronounced with increased applied pressure differential. We hypothesized that this macroscopic effect follows from the response of the mesoscopic foam cells to applied pressure differential. A negative applied pressure differential would cause the closed cells near the surface of the sample to buckle outward, while a positive pressure differential would cause these cells to buckle inward. Once the applied pressure differential was removed, the cells would presumably return to nearly their original shape. However, the long-term application of the hydrostatic pressure could cause the cells to weaken, perhaps by creep, and hence exhibit a propensity to buckle in the same direction when the uniaxial stress was applied. It must be noted that this barreling effect was not uniformly observed; some surfaces did not exhibit the buckling described here, although it was extremely rare for any treated surfaces to exhibit a behavior opposite to that described. Such irreproducibility may result from surface damage of the foam due to effects other than applied pressure differential (i.e. damage due to cutting the foam as discussed below).

Another interesting macroscopic phenomenon we observed was the tendency for foams to develop a curvature when subjected to applied pressure differentials (Fig. 20). The curvature was more pronounced with higher applied pressure differentials. The anisotropy of the stress on the upper and lower curved surfaces was shown in Fig. 21. This phenomenon was finally attributed to damage of the cells near the surface of the foam sample induced by cutting the foam. We hypothesize that the cell wall strength was much weaker for the cut than uncut surfaces. Hence, when the applied hydrostatic load was removed, the cut surfaces recovered much more readily and this produced the observed curvatures.

## V. PROPOSED FUTURE WORK

As with most research, as many questions were raised as were answered by the work presented here. Several extensions of our present research will be proposed in this section. First of all, alternate foam materials will be discussed. Further optical measurements studying density variations of bulk foam samples will be the next topic. Other useful properties such as outgassing and thermal properties will also be addressed.

### A. Alternate Foam Materials

Polystyrene foam was chosen to be the first test material because it is lightweight and it deploys well in a vacuum. Two alternate lightweight materials have also been considered, which are polyurethane foam and aerogels. Different material properties make them potential alternative materials for struts.

Most properties of polyurethane foams are similar to those of polystyrene foams, but they do not deploy as well as polystyrene foams. In general, polyurethane foams (especially high density foams) have better mechanical properties than polystyrene foams. Polyurethane foam density typically ranges from 0.02 to 1 g/cm<sup>3</sup>; <sup>29</sup> polystyrene foams typically range from 0.01 to 0.3 g/cm<sup>3</sup>. <sup>22</sup> Rigid polyurethane foams have been produced by expansion into a vacuum as high as 10<sup>-6</sup> torr. However, at high pressures for the ambient vacuum the foams have reduced mechanical properties. At pressures above 10<sup>-3</sup> torr, polyurethane will not produce sustainable foams. Unfortunately, vacuum conditions in space (due primarily to outgassing) exceed this critical value, limiting use of polyurethane foams in space. Work is presently underway at Thiokol to overcome this problem by using different blowing agents and viscosity mixtures.

Polyurethane foams have already found some other applications in space. Polyurethane foam has been studied in a project of Thiokol Corporation and the University of Alabama at Huntsville. Polyurethane foam was studied and applied in 1963 to the engineering and development of rigidizable shelters for gas in space environments and

solar collectors.<sup>30</sup>

Aerogels were first made from silica in 1930's by S. S. Kistler.<sup>31</sup> By extracting fluid from a wet gel under pressure and at a high temperature, he produced extremely light materials. They possess great potential for applications due to their high porosity (98%), low thermal conductivity, uniform index of refraction, and good acoustic properties.<sup>32</sup>

The delicate aerogel skeleton is built between 2 and 50 nanometers. A phenomenon in aerogels called percolation refers to thermal conductivity by the gel body. In order for percolation to occur, the gel body must be coherent. When studying percolation, aerogels were found to exhibit fractal properties.

Aerogels have very favorable strength-to-weight ratios and are very rigid. Silica aerogels are particularly resistant to damage from atomic oxygen. However, the tendency of aerogels to change their shape when they are subjected to a constant, applied external load makes them subject to creep. Also, silica aerogels are very brittle.<sup>32</sup> One suggestion to minimize this effect is to extract adsorbed water after the aerogel is made.

Aerogels are also expensive and difficult to fabricate (especially in space) using present methods. We were unable to locate a commercial source of aerogels using the Material Referral System & Hotline.

The most common type of aerogel is made of silica. Metal aerogels have also been made. Recently, aerogels have been made from polystyrene.<sup>32</sup> These polystyrene aerogels may overcome many of the negative attributes of aerogels discussed above. Their further development bears close attention.

#### B. Density Uniformity and Cell Structure Studies with Optical Scattering

Our group has begun a series of simple optical measurements that are designed to study the macroscopic and small scale density variations and the structural integrity of foam samples. Some of these experiments will also provide indirect information on the

cellular structure of the foams. The relative density of the foams and the cell wall structure and size distribution have been shown to be the key parameters in understanding the mechanical properties of foams.<sup>23</sup> Density inhomogeneity is key to the yield strength and failure of the composite struts. This set of experiments is based on measurements of the transmission, reflection, and scattering of visible light from bulk and foamed polystyrene (both commercial and Thiokol) samples.

### 1. Adsorption coefficient of bulk polystyrene

This experiment is designed to measure the adsorption coefficient of bulk polystyrene in transmission and the reflection coefficient of a polished surface. Bulk samples have thickness from 50  $\mu\text{m}$  to 1 cm. The transmitted light intensity is modeled by

$$I(x) = (I_0 - I_R) e^{-\alpha x} \quad (49)$$

where  $I_0$  is the incident light intensity,  $\alpha$  is the adsorption coefficient,  $x$  is the sample thickness, and  $I_R$  is the reflected intensity. Another set of experiments varies the surface roughness while maintaining the sample thickness to investigate the dependence of  $I_R$  on surface roughness. These experiments provide a basis with which to compare the optical scattering of foam samples.

### 2. Light transmission and reflection of polystyrene foam

Optical transmission tests of light through rigid foam samples are primarily to study the uniformity of foam density. For typical absorption of light or weakly scattering media, the transmission depends on the sample thickness exponentially. In this case, the optical scattering of foam and bulk samples with the same surface density would be the same, irrespective of the foam density (sample thickness) or cell wall structure. However, Durian et al. found transmission through non-rigid foams with liquid film walls showed an inverse

proportionality to the sample thickness.<sup>33</sup> The proportionality constant can be found by using samples of different thicknesses. This is a “classic signature of diffusive light propagation.” In the limit of sample thickness  $L \gg l^*$  the transport free path and assuming no adsorption, the diffusion model of light predicts

$$T = \frac{5l^*}{3L} \quad (50)$$

where  $l^*$  is also shown to be a measure of (linearly proportional to) the average void size. Thus light transmission studies of foam can also yield information on the cell size distribution.

### 3. Transmission through compressed foams

As discussed above, the diffusive light propagation model predicts that the transmission should depend linearly on the average cell size through the parameter  $l^*$  (see Eq. 50). By contrast, the simple absorption model predicts that transmission depends only on the total amount of polystyrene in the beam, independent of the density or cell size. One way to change the average cell size of foam sample is to compress the foam, although the exact dependence of cell size on compression is not known and is probably not too reproducible. However, measurements of the transmission versus sample compression should clearly distinguish between these two models in a qualitative manner.

The purpose of this experiment is to study the effects of foam density and average cell size on the optical transmission of foam. This information will be used in subsequent experiments to determine foam densities from optical transmission for inhomogeneous foam samples from struts. Samples of several initial densities and thicknesses will be studied.

### 4. Transmission and density contour maps of foam-filled struts

The purpose of these experiments is to use the transmission through cross sections of foam-filled strut samples to determine the cross-sectional density profile. In evaluating the structural integrity and thermal properties of homogeneous foam-filled struts, it is essential to determine the cross-sectional density profiles. A transmission contour map of each 1-cm thick section along a strut can be measured, which can be converted to a three-dimensional density contour map of the strut.

To study the cell size distributions directly, photographs should be taken of each section of the strut to correlate cell size distributions.

An alternate method to measure the transmission of light through the cross sections is the photographic method. Sheets of photographic paper (with the samples sitting on them) are exposed to a uniform light source in controlled dark room conditions. A similar method uses an expanded HeNe laser beam, which is the same size as the cross sections, to take long exposure photographs using a camera or a video camera and a digitizer.

#### 5. Fractal dimension of foams from elastic light scattering

Micrographs of polystyrene foam show that the cell structure can be described by a typical fractal model. The most important factor to characterize a fractal structure is the fractal dimension. The fractal dimension of a material is related to the density, pore size, cell wall thickness, and strength of cell walls (refer to section II. A). If the fractal dimension of foam can be measured, it may allow prediction of important structural properties of foam.

The fractal dimension of materials can be measured by small angle scattering or elastic light scattering. The theories were presented in section II. Small angle x-ray scattering can be used to examine samples with characteristic length of about 1000 Å or less. The difference between small angle x-ray scattering and elastic light scattering is the different sources of light. Elastic light scattering using visible light examines samples with

larger characteristic length scales. Because foam structure behaves like mass fractal, the absolute value of the slope of intensity-to-transferred momentum plot is the fractal dimension.

### C. Thermal Properties

The most important thermal properties of foam as a component of struts applied in space are thermal conductivity and thermal expansion. Thermal conductivity determines the ability to transfer heat from one part of a strut or structure to another. This is essential knowledge to determine what thermal gradients can be established due to unequal heating of different parts of the structure. Thermal expansion can introduce significant stress on the structure. Unequal strains due to thermal gradients can cause thermal stability problems for the structure. Thermal cycling can cause failure due to fatigue. Unmatched thermal expansion of different materials in the composite struts can also lead to weakened or failed bonding between the materials. Colleagues in the USU Mechanical Engineering Department have joined this project to study the thermal stability of foams and composite struts.

In order to have rigid struts of long duration, low thermal conductivity and small thermal expansion are required. The thermal conductivity (under steady conditions) of a homogeneous material is the rate of heat flow through a unit area of a unit thickness per unit temperature gradient in the direction perpendicular to the cross-sectional area. The thermal conductivity can be defined such that

$$k = \frac{x}{A} \times \frac{Q}{T} \quad (51)$$

where  $x$  is the mean specimen thickness,  $A$  is the area of the metered section of the main heater plate, and  $T$  is the steady-state mean temperature difference across the two specimens.<sup>34</sup> The most difficult parameters to determine experimentally are probably the

temperature differences across the specimens T. The correction of T depends on plate-to-specimen thermal contact, on unidirectional heat flow, and on thermocouple calibration. The coefficient of linear thermal expansion should also be measured for the foam by itself and for the composite strut as a whole.

#### D. Outgassing

Outgassing is expected to have a significant influence on the space environment and on the surface characteristics of thermal control coatings and optical surfaces. In our study of the porosity of foam, we found the trapped volume in the foam takes most of the foam volume. The presence of this trapped gas complicates efforts to measure the outgassing due to evaporation or sublimation of the polystyrene itself. Therefore, several experimental methods are proposed to measure the outgassing of foam.

The basic idea is to measure the equilibrium vapor pressure of the foam over a range of temperature. This temperature must be lower than the melting point of foam, which is about 135 to 140 °C at STP for polystyrene foam. The experiment can be performed by placing a block of foam in the pressure box.

One way to measure the outgassing of foam is by controlling the pressure of the system and observing the change of pressure versus temperature. Begin by pumping on the system by a mechanical pump and a diffusion pump for some time to determine the lowest attainable pressure. Record the pressure and temperature until the pressure stabilizes. After the pressure reaches its stable point, shut the vacuum valve and record the equilibrium pressure as a function of temperature. This can be done for a bulk polystyrene sample rather easily. However, gas escaping from the trapped volume in the foam makes this procedure difficult.

Another way to measure the outgassing of foam is to change the temperature of the system. The temperature of the system can be increased or decreased using a temperature controller and an ice bath (an alcohol/dry ice bath or a liquid nitrogen bath). Recording the

pressure-time curve for each temperature determines the equilibrium vapor pressure.

Applying the ideal gas law to these data allows one to calculate the amount of gas released by the outgassing of foam.

Preliminary attempts to measure outgassing were unsuccessful due to escape of gas from the trapped volume. Even after pumping on foam samples for more than 24 hours, the pressure in the box always rose to near 1 atm after 6 to 24 hours.

## VI. CONCLUSIONS

The results of the measured properties of commercial rigid polystyrene foam in this material selection process will be reviewed and the applicability of physical theories will be discussed. The selection process will be evaluated by the applicability on other lightweight materials presented and on other components of the struts. The improvement of the material selection will also be proposed.

Basic properties of a simple uniform polystyrene foam (e.g. density, total and available porosity, permeability, surface area, isotropicity, and cell size and cell wall thickness distributions) have also been studied. During material preparation and the tests performed, external forces change the foam cells from isotropic to anisotropic, which can be characterized by open-cell models. Among the chosen experimental methods for studying density, the gravimetric method gives the best result. The pressure-volume curve gives the result with smallest uncertainty in the porosity measurements. High values of total porosity show that polystyrene foam is a highly porous material. Low permeability proved the cell structure of polystyrene foam was essentially closed. Based only on density consideration, foams fit the requirement of being a lightweight material.

Standard compression and deflection tests were performed. The stress-strain curves and related mechanical properties of foams treated under different pressure differentials were studied. In the series of experiments designed to study the foam mesoscopic structure, significant effects in Young's modulus, relative elastic collapse stress, and ultimate strength were observed when the pressure differential exceeded 2 atm. Another important phenomenon found was the barreling of foam samples under positive and negative pressure differentials, which relates to the Poisson's ratio. We also observed the curvatures of a foam sample when subjected to applied pressure differentials in the pressure box. The anisotropy of the stress on the cut and uncut surfaces showed the damage of the external cells in the sample preparation process. Thus the pressure differential in the foam deployment

procedure was found to be the essential aspect of determining the strength of struts.

Most of our results were consistent with those reported by previous investigators and were modeled well by the cellular structural model of open-cell foams. We can conclude that the mechanical properties of the untreated foam samples were acceptable for our proposed application as materials for struts for innovative space structures.

Two alternative lightweight materials, polyurethane foam and aerogels, have been considered. The evaluation methods and criteria need to be adjusted when they are applied to polyurethane foams and aerogels. Different mechanical properties and constraints of these two materials mentioned in section V. A. limit the applied pressure to below  $10^{-3}$  torr. At high pressures, polyurethane has reduced mechanical properties, and aerogels are subjected to creep. Therefore, fine pressure measuring devices need to be built to find the critical value of the pressure differentials.

This work was originally motivated by applications of foam as an inflating agent and structural component of fiber-epoxy composite tubular struts to be used in innovative space structures. Since the tube is highly porous and rigid, the evaluation methods of polystyrene foam presented may be appropriate for other components of the struts such as the composite tube. However, the composition of the tube needs to be investigated.

The evaluation process can be improved by tracing the manufacturing procedure of the commercial polystyrene foam (for the impact on density inhomogeneity and surface damages) and by closely monitoring the effects from the pressure differentials.

## REFERENCES

1. L. J. Gibson, and M. F. Ashby, Cellular Solids Structures and Properties, (Pergamon Press, New York, 1988), pp. 12-35.
2. S. C. Warburton, A. M. Donald, and A. C. Smith, Structure and Mechanical Properties of Brittle Starch Foams, (Chapman & Hall, New York, 1992), pp. 1469-74.
3. R. W. Morse, "Fluid-flow properties of porous media and viscosity of suspensions," American Institute of Physics Handbook, (Mc-Graw Hill, New York, 1957), pp. 2-179.
4. J. Bear, Dynamics of Fluids in Porous Media, (Elsevier Publishing, New York, 1972), p. 303.
5. C. R. Eugene, "Structure and properties of porous materials," Flow of Fluids through Porous Materials, (Reinhold Pub. Co., New York, 1961), pp. 1-21.
6. F. D'Orazio, J. C. Tarczoz, and W. P. Halperin, "Application of nuclear magnetic resonance pore structure analysis to porous silica glass," J. of Appl. Phys., 65, N2, 742-751 (1989).
7. K. Munn, and D. M. Smith, "An NMR technique for the analysis of pore structure: Numeral inversion of relaxation measurements," J. of Colloid. and Interface Sci., 119, N1, (1987).
8. U. Oxaal, M. Murat, F. Boger, A. Aharony, J. Feder, and T. Jossang, "Viscous fingering on percolation clusters," Nature, 329, 32-373 (1987).
9. M. D. Fuller, and P. M. Gammell, "Ultrasonic characterization of porosity in composite materials by time delay spectrometry," Review of Progress in Quantitative Nondestructive Evaluation, 6B, 1157 (1987).
10. J. Papadakis, "Ultrasonic attenuation due to grain scattering in polycrystalline metals," J. of the Acoustical Society of America, 37, 711 (1965).
11. C. F. Quate, "Acoustic microscopy," Physics Today, 38, 34-40 (1985).
12. H. D. Bale, and P. W. Schmidt, "Small-angle x-ray-scattering investigation of

- submicroscopic porosity with fractal properties," *Physical Review Letters*, 53, N6, 596-599 (1984).
13. D. Stauffer, Introduction to Percolation Theory, (Taylor and Francis Inc., London, 1985), pp. 61-78.
  14. J. C. Kimball, and H. L. Frisch, "Diffusion through foams and fractal-like cellular solids," *Phys. Rev. A*, 43, N4, 1840-1848, (1991).
  15. B. Mandelbrot, Fractals, Form and Dimension, (Freeman, San Francisco, 1977).
  16. NATO Advanced Study Institute, "On growth and form: fractal and non-fractal patterns in physics," H. E. Stanley and N. Ostronsky, eds. (Dordrecht, Boston, 1986), pp. 145-162.
  17. P. W. Schmidt, "Small-angle scattering studies of disordered, porous and fractal systems," *J. Appl. Cryst.*, 24, 414-435 (1991).
  18. J. Martin, and A. Hurd, "Scattering from fractals," *J. of Appl. Cryst.*, 20, 61-78 (1987).
  19. D. W. Schaefer, J. E. Martin, P. Wiltzius, and D. S. Cannell, "Fractal geometry of colloidal aggregates," *Phys. Rev. Lett.* 52, 2371 (1984).
  20. H. Ehrenehich, D. Turnbull, and S. H. Liu, "Fractals and their applications in condensed matter physics," Solid State Physics, 39, (Academic Press, New York, 1986), pp. 207-267.
  21. P. S. Theocaris, "The elliptic paraboloid failure criterion for cellular solids and brittle foams," *Acta Mechanica*, 89, 94 (1991).
  22. A. R. Ingram and J. Fogel, "Polystyrene and related thermoplastic foams," Plastic Foams, V. 2, K. C. Frisch and J. H. Saunders, eds. (Marcel Dekker, Inc., New York, 1973), pp. 525-638.
  23. M. F. Ashby, "The mechanical properties of cellular solids," *Metallurgical Transactions A*, 14A, 1757 (1983).

24. E. Baer, Engineering Design for Plastics, (Chapman & Hall, New York, 1964).
25. S. Swyngedau, A. Nussinovitch, I. Roy, M. Peleg, and V. Huang, "Comparison of four models for the compressibility of breads and plastic foams," J. of Food Sci., 56, N3, 757 (1991).
26. D. M. Young, and A. D. Crowell, Physical Adsorption of Gases, (Butterworths, Washington, 1962).
27. J. Bear, D. Zaslavsky, and S. Irmay, "Physical principles of water percolation and seepage," (UNESCO, Paris, 1968).
28. Micromeritics Instrument Corporation, "Micro report, first quarter," 3, N1 (1992).
29. J. K. Backus, and P. G. Gemeinhardt, "Rigid urethane foams," Plastic Foams, V. 2, K. C. Frisch and J. H. Saunders, eds. (Marcel Dekker, Inc., New York, 1973), pp. 451-524.
30. S. Allinkov, and S. Schwartz, "Fabrication of foamed polyurethane structures in a space equipment," Symposium on Effects of Space Environments, (Air Force Report No. AF 7381, 1963), pp. 1-21.
31. J. Fricke, "Aerogels," Sci. Am., 92-97 (1989).
32. D. Erickson, "Relative lightweights," Sci. Am., 128 (May 1992).
33. D. J. Durian, D. A. Weitz, and D. J. Pine, "Multiple light-scattering probes of foam structures and dynamics," Science, 252, 686-688 (1991).
34. L.L Sparks, Thermal Conductivity of a Polyurethane Foam from 95 K to 340 K, (National Bureau of Standards Report No. NBSIR 88-3086, 1964), pp. 1-20.